



저작자표시-비영리-변경금지 2.0 대한민국

이용자는 아래의 조건을 따르는 경우에 한하여 자유롭게

- 이 저작물을 복제, 배포, 전송, 전시, 공연 및 방송할 수 있습니다.

다음과 같은 조건을 따라야 합니다:



저작자표시. 귀하는 원저작자를 표시하여야 합니다.



비영리. 귀하는 이 저작물을 영리 목적으로 이용할 수 없습니다.



변경금지. 귀하는 이 저작물을 개작, 변형 또는 가공할 수 없습니다.

- 귀하는, 이 저작물의 재이용이나 배포의 경우, 이 저작물에 적용된 이용허락조건을 명확하게 나타내어야 합니다.
- 저작권자로부터 별도의 허가를 받으면 이러한 조건들은 적용되지 않습니다.

저작권법에 따른 이용자의 권리는 위의 내용에 의하여 영향을 받지 않습니다.

이것은 [이용허락규약\(Legal Code\)](#)을 이해하기 쉽게 요약한 것입니다.

[Disclaimer](#)

Ph.D. Dissertation of Engineering

**Microfluidic *in vitro* model of
3D Tumor Vascular Networks for
Cancer Immunotherapy Screening**

면역세포치료제 및 항암제 평가를 위한
미세유체소자기반 3차원 체외 암-혈관 모델

February 2020

**Graduate School of Engineering
Seoul National University
Department of Mechanical Engineering**

Jiyoung Song

면역세포치료제 및 항암제 평가를 위한
미세유체소자기반
3차원 체외 암-혈관 모델

**Microfluidic *in vitro* model of 3D Tumor Vascular
Network for Cancer Immunotherapy Screening**

지도교수 전 누리

이 논문을 공학박사 학위논문으로 제출함
2020년 10월


서울대학교 대학원
기계항공공학부
송지영

송지영의 공학박사 학위논문을 인준함
2020년 12월

위원장 : 이윤석 (인) 

부위원장 : 전누리 (인) 

위원 : 신용대 (인) 

위원 : 도준상 (인) 

위원 : 김홍남 (인) 

Ph.D. Dissertation of Engineering

**Microfluidic *in vitro* model of
3D Tumor Vascular Networks for
Cancer Immunotherapy Screening**

면역세포치료제 및 항암제 평가를 위한
미세유체소자기반 3차원 체외 암-혈관 모델

February 2020

**Graduate School of Engineering
Seoul National University
Department of Mechanical Engineering**

Jiyoung Song

Abstract

Microfluidic *in vitro* model of 3D Tumor Vascular Networks for Cancer Immunotherapy Screening

Jiyoung Song

Department of Mechanical Engineering

College of Engineering

Seoul National University

Colorectal cancer is second most common cause of cancer death. Numerous approaches for the treatment of colorectal cancer have been proposed while there is still absence of breakthrough therapy designation. Cancer immunotherapy holds great promise recently, however, the exact mechanism of the interaction between immune cells and tumor cells remains poorly understood. Moreover, it is important to consider blood vessel in colorectal cancer study since the blood flows from colon to liver causing distant metastasis. Despite the importance of blood vessel in tumor microenvironment, current models have missed the tumor vascular networks.

This thesis describes an injection molded platform to mimic the complex

three-dimensional tumor vascular networks for evaluating immune cell behavior in tumor microenvironment(TME). Our platform consisting of 28 wells enabled simple and high-throughput screening. We characterized the aberrant tumor vasculature according to colorectal cancer subtypes and confirmed an increased permeability of blood vessels, which is a major feature of aberrant tumor vasculature. We also evaluated natural killer (NK) cell infiltration and cytotoxicity according to CMS subtypes. NK cells showed higher cytotoxicity in CMS 1 type colorectal cancer compared to the others and this result is correspondence with physiological theory of existence of intratumoral immune cells.

In the meantime, the subtype classification of macrophages and the role of each subtype in various carcinomas including colorectal cancer have been studied for decades. However, consistent results on the role of tumor associated macrophages and their relationship with clinical prognosis have not been defined yet. In this thesis, we verified the effect of macrophage on not only tumor but also tumor microenvironment according to their subtypes. We confirmed M1 macrophage inhibit the tumor progression whereas M2 macrophage enhance.

Our results showed physiological relevance of our platform and potential of our platform in both chemotherapy and immunotherapy since perusable

vascular networks provided a route for the delivery of lymphocytes or molecules from a distance site to the tumor site. We hope our *in vitro* tumor vascular networks model to be used for better understanding of cancer and cancer treatment.

Student Number: 2016-35810

Contents

Abstract

List of tables

List of figures

Chapter1.

Introduction.....1

- 1-1. Feature of colon cancer and metastasis
- 1-2. Characteristics of tumor-vasculature
- 1-3. Micro-engineered in vitro tumor-micro vessel models
- 1-4. Study of immune cell in microfluidics
- 1-5. Motivation and objectives

Chapter 2. 3D Vascular networks co-cultured with various types of colorectal cancer cells for validation of natural killer cell cytotoxicity.....15

- 2-1. Introduction
- 2-2. Materials and methods
- 2-3 Results & Discussion
 - 2-3-1. Device working principle
 - 2-3-2. Tumor vessel formation.
 - 2-3-3. Effect of culture medium condition on tumor-vasculature
 - 2-3-4. Colorectal cancer cell concentration optimization for tumor-vasculature
 - 2-3-5. Permeability measurement of tumor-vasculature
 - 2-3-6. Characterization of colorectal cancer lump in tumor-vasculature
- 2-4. Summary

Chapter 3. The effect of tumor-associated macrophage (TAM) on tumor microenvironment (TME) in microfluidic device.....66

3-1. Introduction

3-2. Materials and methods

3-3 Results & Discussion

3-3-1. Experimental design and functional validation of tumor-vasculature

3-3-1. The effect of macrophage condition medium(CM) on colorectal cancer

3-3-2. The effect of macrophage condition medium(CM) on tumor microenvironment(TAM)

3-3-3. The effect of macrophage on blood vessel

3-4. Summary

4. Conclusion.....82

References

요약

List of tables

Table 1. CMS classification of CRC cells and MSI/MSS status. Genetic information of CRC cells.

List of Figures

Figure 1. The characteristic of colon cancer.

Figure 2. The characteristic of tumor vasculature.

Figure 3. Micro engineered tumor vessel models.

Figure 4. Recent study of immune cells in microfluidics.

Figure 5. Objective of research. Perusable tumor microvessel for evaluation of cancer-immunotherapy \

Figure 6. CMS classification and MSS/MSI status of CRC cells. MSI status was labelled with red.

Figure 7. Principle of liquid patterning in rails.

Figure 8. Actual image of device and illustration of hydrogel patterning.

Figure 9. Actual image of the channel hydrogel patterning and experimental configuration of the microfluidic platform.

Figure 10. Stromal cell type dependent Angiogenesis and vasculogenesis

Figure 11. Confocal image of tumor vessel formation.

Figure 12. The effect of culture medium condition on tumor vasculature.

Figure 13. The effect of EGM-2 supplemented with 20% FBS on tumor vasculature.

Figure 14. The effect of CRC concentration for tumor vasculature.

Figure 15. The effect of HCT 116 cell concentration on tumor vasculature.

Figure 16. Morphological differences and size distribution of CRC cells.

Figure 17. Permeability measurement of normal and tumor vasculature.

Figure 18. Permeability measurement tumor vasculature.

Figure 19. Cytotoxic activity of NK cells on a 2D culture.

Figure 20. 3D confocal image of NK cytotoxicity and infiltration in 3D tumor vasculature.

Figure 21. 3D confocal image of NK cytotoxicity to various CRC cells.

Figure 22. Number of NK cells extravasated and death rate of both (A) HT29 and (B) SW480 during live-cell imaging.

Figure 23. The effect of NK cell number on cytotoxic activity.

Figure 24. CMS classification of CRC cells.

Figure 25. Previous study of immune cells in microfluidics.

Figure 26. Macrophage differentiation.

Figure 27. The effect of macrophage on CRC cells

Figure 28. The effect of macrophage on HUVEC.

Figure 29. SEM image of extracellular matrix and quantification.

Figure 30. Western blot of Matrix metalloproteinase(MMP) MMP2 and MMP9.

Figure 31. The effect of macrophage on vascular permeability.

Figure 32. Confocal image of tight junction expression.

Figure 33. Cytokine assay of cancer monoculture and tumor vessel co-culture condition. Fewer types of inflammatory cytokines were detected.

Chapter 1. Introduction

The time consumption for a new drug development today is the same as 50 years ago due to the inefficiency of current preclinical drug evaluation models. Moreover, the cost for development of new drugs has increased during a few decades due to the absence of ideal drug evaluation models. A phylogenetic gap between human and animal model is the major disadvantage of conventional preclinical models. Also, petri dish based two-dimensional culture systems have showed limited correlation with in-vivo system.

Microfluidic technology has evolved as a promising alternative to conventional preclinical models. Micro-engineered structures enable us to co-culture different cells in three dimensional culture system. This 3D *in vitro* culture models improved physiological relevance by mimicking the complex structure of tissue. Especially, blood vessels are existed all part of our body, supplying nutrients and eliminating waste from tissue. Therefore, it is necessary to recreate *in vitro* tissue models with microvascular endothelial cells(EC).

Meanwhile, EC that composed of tumor microenviroment interplays a key role by secreting various growth factors and cytokines for tumor progression. Tumor also induced the angiogenesis by releasing the growth factor such as vascular endothelial growth factor- A (VEGF-A) to supply oxygen and nutrient and

eliminate acidic product such as lactic acid. This microvessel surrounding the tumors has distinct characteristic. This tumor vascular network is often called “aberrant vasculature”. Therefore, we developed micro-engineered vascularized tumor arrays that composed of various types of colorectal cancer cells and perusable microvessel. The device is open microfluidic capillary system. The concept of “open microfluidic” system is part of microfluidic techniques, it utilized capillary force and interaction between hydrophilicity of surface and aqueous droplets. Our group recently proposed rail guided injection molded microfluidic techniques. By altering the ratio of width and height of the rail, we optimized the successful liquid patterning condition. Later then, we modified the rail structures and raised the number of samples per device to 28. Our device was fabricated by injection molding techniques using polystyrene, became to make a single chip the more and the faster. High-throughput screening helps us optimizing the culture condition for tumor vascular system.

In chapter 2, we reconstructed 3D tumor vascular networks for evaluation of the drug or immune cell therapy *in vitro*. We optimized the culture condition and medium condition for aberrant vasculature. We facilitated various types of colorectal cancer cells, since colorectal cancer cells showed different feature according to their genomic characteristics. We quantified the feature of vessels such as vessel area and length and the number of junction to optimize the culture

condition. Also, we analyzed the morphological characteristic of tumors. We did not deal with the physiological relevance between the morphology of tumor and anti-tumor drugs here. Instead, we validated the cytotoxic activity of Natural Killer(NK) cells according to the consensus molecular subtypes(CMS) of colorectal cancer. Recent research trends in colorectal cancer studies underline that considering CMS with distinct molecular and genomic features is more important. This categorization helps us understand immune cell infiltration and molecular immunological features of CRCs.

In chapter 3, we validated the effect of tumor associated macrophage(TAM) on tumor vascular networks. We observed the opposite effect of macrophage on tumor microenvironment. M1-phenotype and M2-phenotype has been known to have opposite behavior on cancer. M1 macrophage secretes pro-inflammatory cytokines such as TNF- α , IL-1 β , and CXCL9, whereas M2 macrophage secretes anti-inflammatory cytokines. M2 macrophage is also involved in matrix remodeling and tissue repair by secretion of MMPs, TGF- β , and IL-10. It seems to have only M1 macrophage in tumor site, however, both M1 and M2 macrophages are observed in clinical surgery. Also, the population ratio between 2 phenotypes varies from patient to patient. Therefore, it is necessary to develop 3D tumor vasculature model in vitro to validate the effect of macrophage on tumor. Here, we proposed our in-vitro tumor-vascular models to evaluate the role of macrophage on not only tumor

progression but also the tumor microenvironment. Our model is expected to use as a preclinical model to evaluate the colorectal cancer immunotherapy. We hope our device to increase the success rate of colorectal cancer immunotherapy with better understanding of interaction between macrophage and tumors.

1-1. The feature of colon cancer and metastasis

Colorectal cancer (CRC) is one of the highly metastasis carcinoma owing to their anatomical characteristics. The most common form of distance metastasis is liver since the blood flows from colon to liver via portal vein (Fig. 1) Tumor cells in early stage grow up in their size and intravasate to blood vessel or lymph node. This circulating tumor cells (CTC) extravasates to liver. Up to 70 percent of people with colorectal cancer also develop metastatic liver cancer. Most of all, prognosis for these patients with metastatic liver cancer tends to be poor. Their survival rate is approximately 11% for 5 years. Therefore, it is necessary to consider the tumor-microenvironment including the microvessel.

[

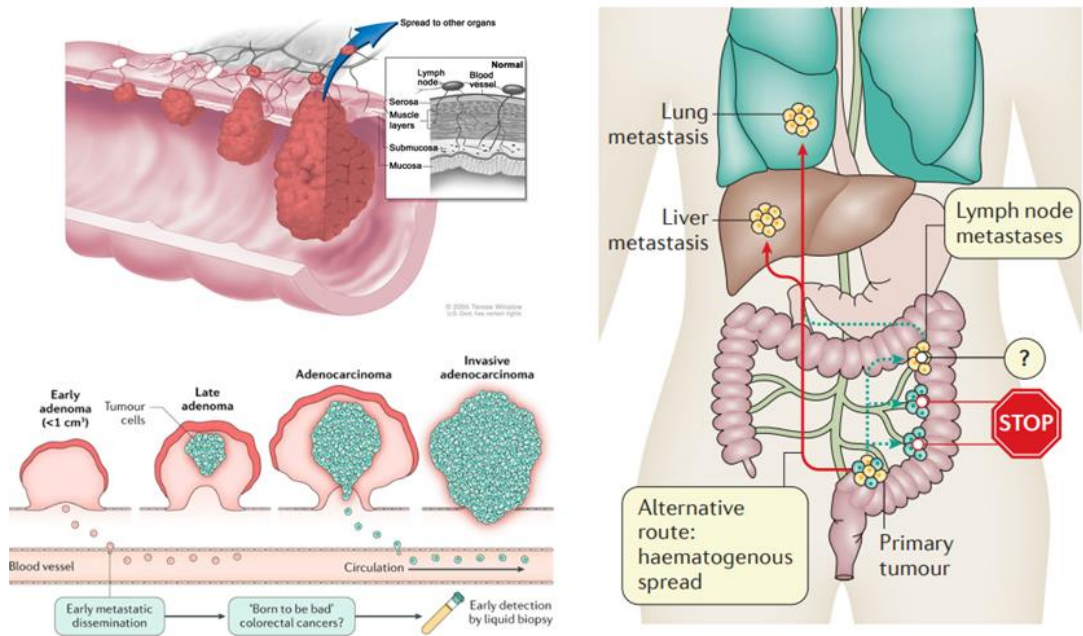


Figure 1. The characteristic of colon cancer. The most common site of distance metastasis of colon cancer is liver since the blood flow from colon to liver via portal vein.

1-2. The characteristics of tumor-vasculature

This collapsed and narrowed abnormal blood vessels are the characteristic of tumor vessels. (Fig. 2) The basement membrane surrounding the vessels are collapsed and pericyte and vascular smooth muscles are functionally disrupted. Most of all, there are the lack of the endothelial cells that composed of lumens. The disorganized and abnormal vessels have several distinct features. Since they are collapsed and narrowed lumen they failed to deliver the oxygen and nutrients to the tissue. Consequently, they microenvironment surrounding the tumor becomes acidic. Moreover, the microvessels near tumor are leaky. This leaky vessel resulted in high interstitial flow pressure. We reconstructed the tumor microvessel, considering this distinct features.

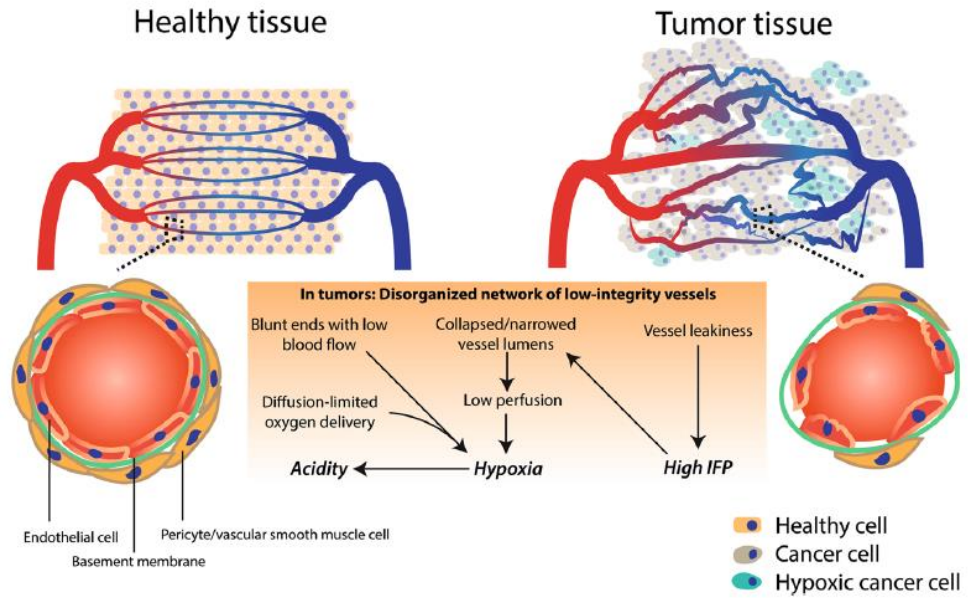


Figure 2. The characteristic of tumor vasculature. Collapsed and winding lumen formation and leakiness are the major feature of tumor vessel.

1-3. Micro-engineered in vitro tumor-micro vessel models

There have been many in vivo and in vitro models to evaluate newly developed anti-tumor drugs, however, phylogenetic gap between human and animal models and a lack of similarity between in vivo and 2D culture system are the major disadvantage of conventional preclinical models. As micro technology has evolved, there have been many approaches proposed to develop experimental model for tumor vessel. (Fig. 3)

In the early stage, Zervantonakisa et al. developed endothelial channel by forming endothelial monolayer on the wall of hydrogel. Then they loaded the fibrosarcoma cells and induced migration by TNF- α stimulation. The migrated tumor cells attached and intravasated the lumen. Advanced model has developed to create more complex tumor microenvironment. Sobino *et al.* have created 3 layered microfluidic device for tumor-vascular model. This device includes large medium reservoirs to induce interstitial flow by hydrostatic pressure. Recently, Haase *et al.* have developed microvessel with tumor spheroid in microchannel. They culture the tumor spheroid for 7 days and mixed with endothelial cell, fibroblast in fibrin gel. They also measure the vascular permeability and intracellular uptake of Taxol. Ko *et al.* also have created injection molded vascularized tumor in microfluidics. He contributes to increase the throughput of experiment.

Meanwhile, open microfluidic techniques have developed during last few years. Open microfluidics is a part of microfluidic techniques. Microfluidic facilities channels for liquid

patterning, on the other hands, open microfluidics uses rail guide to fill the channel. The hydrophilicity of surface and capillary force are the major principle to move flows. Since we used open microfluidic techniques, it is easy to pattern hydrogels within channels without any additional equipment or training. Therefore, we were able to load the hydrogel in microchannel easily, and anyone can create tumor-microvessel system at once.

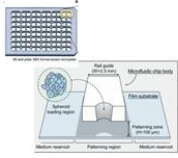
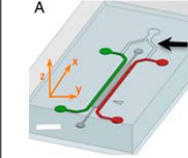
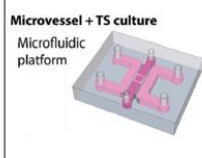
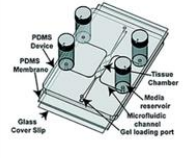

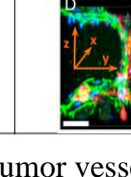

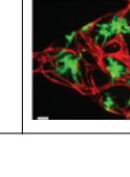
	<i>Ko et al.</i>	<i>Jeon et al.</i>	<i>Haase et al.</i>	<i>Sobrino et al.</i>
Device Schematics			Microvessel + TS culture 	
Representative result				

Figure 3. Micro engineered tumor vessel models.

1-4. Study of immune cell in microfluidics

As Cancer immunotherapy rises as an alternative cancer treatment in the past decade, there has been many researches in interaction of tumor and immune cells in microfluidics. (Fig. 4) A. Boussommier-Calle *et al.* have created microvessel in hydrogel and introduced cancer cells into the vessel. The more cancer cells extravasated while they loaded with monocytes. Bi *et al.* have developed the system to examine the cancer cell migration according to the existence of monocytes(THP-1). Ayuso *et al.* have developed the experiment to evaluate NK cytotoxicity against tumor spheroids.

Those experiment have developed study of cancer immunotherapy in microfluidics. However, there is the absence of tumor vasculature co-culture system.

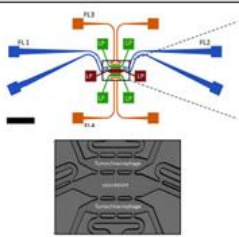
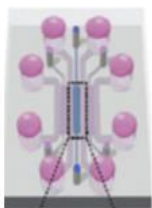
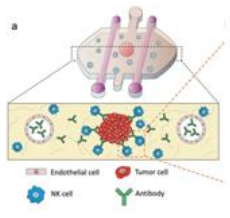
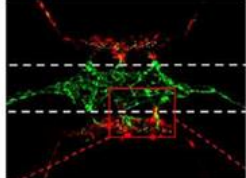
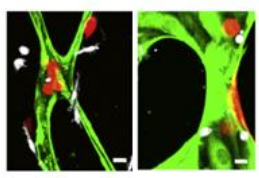
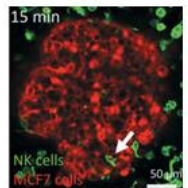
	Bi <i>et al.</i>	A. Boussommier-Calle <i>et al.</i>	Ayuso <i>et al.</i>
Device Schematics			
Representative result			

Figure 4. Recent study of immune cells in microfluidics.

1-5. Motivation and objectives

There is an urgent need for preclinical drug test model in vitro, since conventional in vivo experimental model cannot reflect the phylogenetic gap between human and animal. Moreover, the poor similarity between 2 dimensional culture and in vivo makes it difficult to rely on the result. Recently, numerous models have been proposed to study tumor microenvironment. However, there is still absence of in vitro models that recapitulating actual tumor-microenvironment in aspect of co-culturing tumor microvessel.

In the meantime, cancer-immunotherapy has become promising candidate as a next generation of cancer treatment. Since immune cells target the tumor cells and have no effect on the other cells, the side effects of treatment are also less than the traditional treatment. However, still there is poor understanding of interaction between immune cells and tumor. Therefore, we proposed microfluidic device that recapitulating 3D tumor vasculature for evaluation of cancer immunotherapy. (Fig.

5)

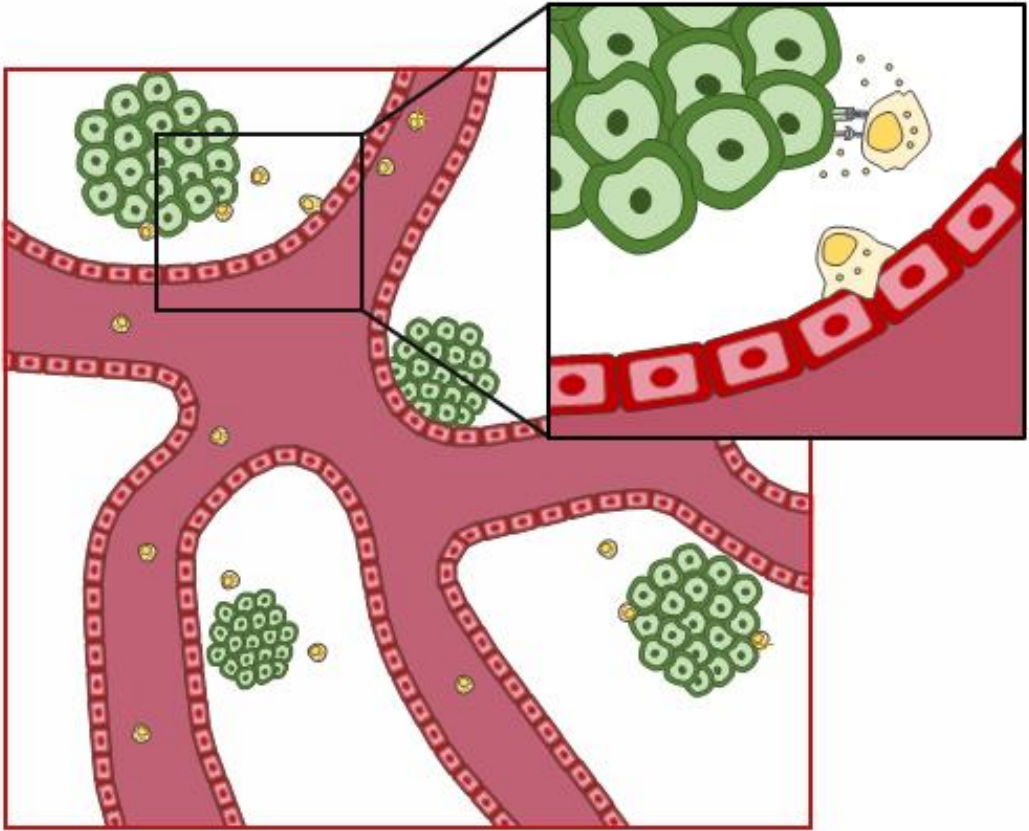


Figure 5. Objective of research. Perusable tumor microvessel for evaluation of cancer-immunotherapy

Chapter 2

3D Vascular networks co-cultured with various types of colorectal cancer cells for validation of natural killer cell cytotoxicity

2-1. Introduction

Colorectal cancer (CRC) is the second leading cause of cancer-related deaths worldwide due to a recurrence with metastasis and poor prognosis. Hence, CRC has been actively studied to reveal its cellular and genetic mechanisms to identify new targets for cancer therapies over the past several decades. Plenty of traditional *in vitro* CRC models based on two-dimensional culture systems or animal models have accelerated the development of anti-cancer drugs, yet the limitations of the models remain concerning the absence of three-dimensional (3D) tumor microenvironment (TME) such as a vascular network, stromal cells, and extracellular matrix (ECM). *In vitro* 3D tumor vasculature models to study tumor dynamics have been considered important since tumors continuously interact with surrounding vascular networks. Therefore, recent studies related to tumors and vascular networks in microfluidic devices have been proposed; however, their low-

throughput and laborious experimental design including an external fluid pump make it impractical to use for clinical purposes. Meanwhile, cancer immunotherapy holds great potential as an efficacious treatment for different types of cancer. There have been numerous attempts to treat cancer using dendritic cells, engineered T cells, and NK cells, however, only a few patients showed beneficial responses to the therapies thus far. Therefore, there is an urgent need for improved *in vitro* models including the complex interplay between tumors and their surrounding microenvironment.

Herein, we developed a 3D microfluidic platform for a better understanding of aberrant characteristics of tumor vasculature and cytotoxic lymphocyte infiltration. Aberrant tumor vasculature completely differs from the normal vasculature and has distinct features such as a chaotic flow pattern or high permeability. This disorganized and immature vasculature hinders to deliver target drugs or immune cells to the tumor site, resulting in reduced success rates of therapies. By altering cancer cell seeding density and the medium composition, we succeed to optimize the culture condition for constructing the tumor vasculature without any extra equipment for continuous flow. The perfusability of vascular networks was confirmed by permeability tests, which ensured that molecules or NK cells were later allowed to travel via the vascular networks. Additionally, the cytotoxic activity of NK cells was evaluated against different subtypes of CRC cell lines,

demonstrated as one of the possible applications using this platform. The results showed the potential of our platform in both chemotherapy and immunotherapy since perfusable vascular networks provided a route for the delivery of lymphocytes or molecules from a distance site to the tumor site. We expect that our platform could be further considered as a powerful tool for drug screening in preclinical stages.

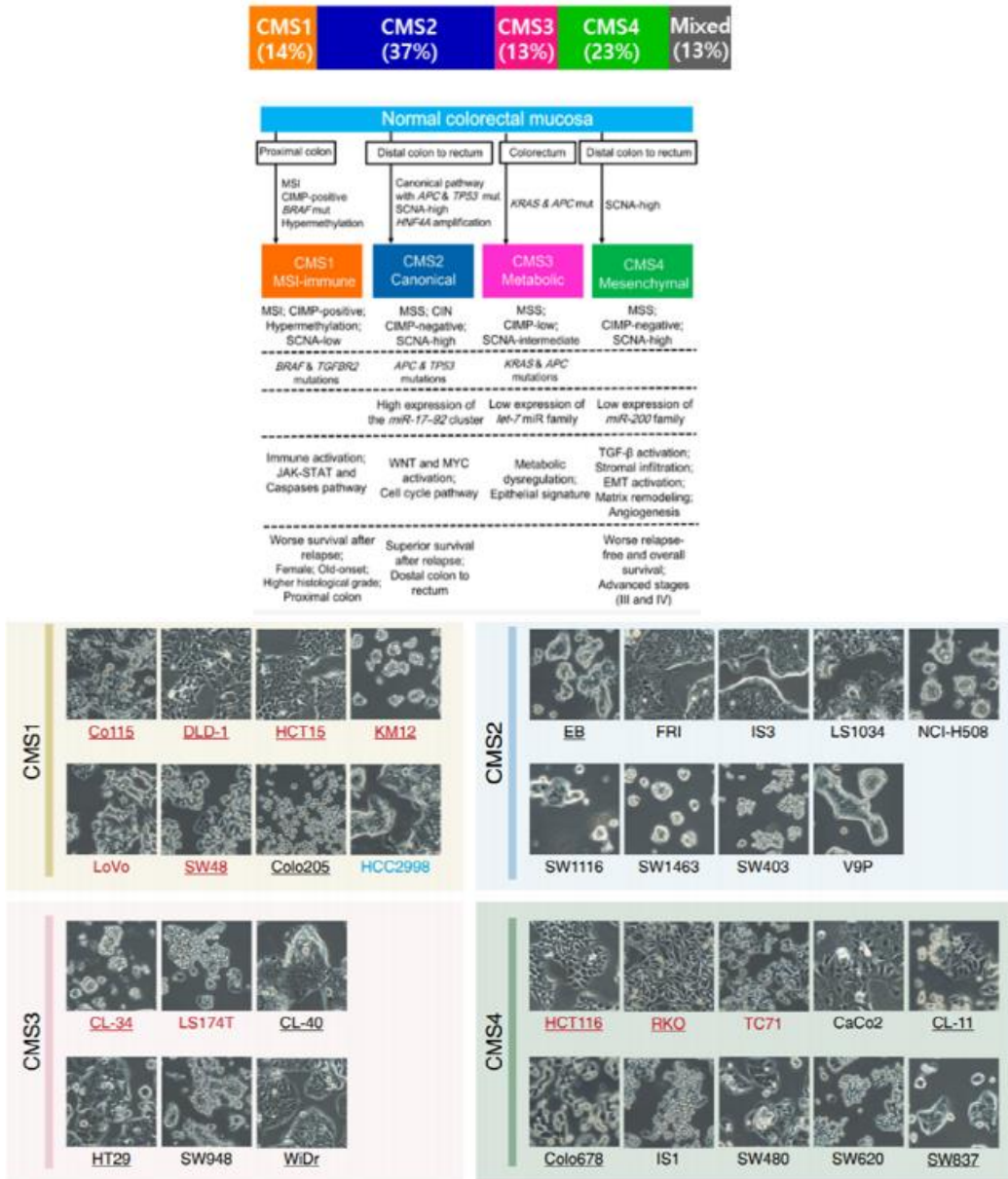


Figure 6. CMS classification and MSS/MSI status of CRC cells. MSI status was labelled with red.

2-2. Material and Methods

2-2-1. Design and fabrication of device

Aluminum alloy mold was fabricated by machining and polishing process. Polystyrene (PS) injection molding was performed at 130 tons of clamping force with 55 bar of injection pressure for 15 seconds. The nozzle temperature was 220°C. The injection molded plastic chips underwent surface oxygen plasma treatment of 5.00e-1 Torr, 50 W for 1 min, then bonded to substrate film.

2-2-2. Cell culture

Human umbilical endothelial cells (HUVECs; Lonza, Swiss) were cultured in endothelial growth medium 2 (EGM-2; Lonza). Lung fibroblasts (LFs; Lonza) were cultured in fibroblast growth medium 2 (FGM-2; Lonza). Colorectal cells were cultured in RPMI medium supplemented with 10% of fetal bovine serum (FBS) and 1% penicillin-streptomycin (PS). NK cells were cultured in RPMI medium supplemented with 10% of FBS, 1% of PS, and an extra 2nM of L-glutamine. Interleukin-2 and interleukin-15 were also added in the medium immediately before incubation.

2-2-3. Cell seeding

HUVEC, LF, and CRC cell suspensions were prepared and mixed with fibrinogen solution (Final concentration of 2.5mg/ml, Sigma, USA) and bovine thrombin (0.5 Unit/ml, Sigma). The concentrations for each cell type were 6×10^6 per mL for HUVEC, 2×10^6 per mL for LF, and 0.1-0.3 10^6 per mL for CRCs, respectively. 0.9 μ L of this acellular mixture was then introduced to the central channel. Capillary forces led this solution into the guide rail. The first gels were incubated for 6 min to undergo polymerization. Then 3 μ L of HUVEC suspension at a concentration of 3mil/ml was loaded into both side channels. The device was tilted 90° for 15 min to attach the HUVECs to the surface of the fibrin gel. Then, 100 μ l of fresh medium was introduced to all the medium channels. EGM-2 supplemented with 10% or 20% FBS was used while the cells were cultured in the device. The device was incubated at 37 °C and 5% CO₂, and media was changed every day for 5 days.

2-2-4. Immunocytochemistry

The samples were fixed with 4% (w/v) paraformaldehyde (Biosesang, Korea) in PBS (Gibco, USA) for 15 min and permeabilized with Triton X-100 0.1% (v/v) in PBS for 15 min. Endothelial cell (EC)- specific staining was performed using 488 fluorescein-labeled Ulex Europaeus Agglutinin I (Vector, UK), which was prepared at a 1:1000 ratio of dye in BSA for 12 h at 4 °C. Tumor tissue-specific surface staining was done with Alexa Fluor 488 tagged anti-epithelial cell adhesion

molecule (EpCAM, CD326; Biolegend, USA) using a dye diluted in BSA at a 1 : 200 ratio.

2-2-5. Live imaging

Live cell imaging was performed using a Ti2-eclipse inverted microscope (Nikon Eclipse Ti, Japan) with NIS elements software (Nikon, Japan). The samples were stained with lectin and EpCAM 3 hours prior to imaging. NK cells were labelled with CellTrace™ Far Red Cell Proliferation Kit (Thermo fisher, C34572) in serum-free RPMI and incubated for 30 min. Then, they were neutralized with the same amount of serum-included RPMI medium as the serum-free RPMI and were incubated for another 5 min. The concentrations of NK cells at 0.05 mi/mL and 0.1 mi/mL were used for NK cell cytotoxicity assays. After NK cells were introduced into the vessels, time-lapse live-cell imaging was performed for 22 hrs.

2-2-6. Image analysis

Confocal images were analyzed using Image J. Confocal, and 3D images were converted to 2D images by z-projection. Afterwards, the ROI was cropped and converted to a binary mask. The binary mask image was acquired using threshold. All the measurements including those in the vessel area and cancer area were performed automatically. The number of junctions in tumor vasculature was

analyzed using Angiotool. (National Cancer Institute)

2-2-7. Statistical analysis

Prism (GraphPad, USA) was used for statistical comparison. Ordinary one-way ANOVA with multiple comparisons was used to obtain the statistical value. The Threshold for statistical significance set t *p < 0.1. **p < 0.01; ***p < 0.001; ****p < 0.0001; and ns (not significant). The standard error of the mean (SEM) was presented in error bars.

Cell line	MSS/MSI	CMS type	KRAS	BRAF	TP53	APC
HT29	MSS	CMS3	WT	V600E/T119S	R273H	G263G
SW480	MSS	CMS4	G12V	WT	R273H/P309S	Q1338*
SW620	MSS	CMS4	G12V	WT	R273H/P309S	Q1338*
HCT116	MSI	CMS4	G13D	WT	WT	WT
SW48	MSI	CMS1	WT	WT	G61W	R2714C
LoVo	MSI	CMS1	G13D/V14A	WT	WT	R2816Q

Table 1. CMS classification of CRC cells and MSI/MSS status. Genetic information of CRC cells.

2-3. Results and discussion

2-3-1. Device working principle

The injection molded plastic chip is composed of 3 parallel rails side by side designed to pattern different cell types. (Fig. 7) Each rail can be used for cell seeding, which enables direct cell-cell contact or the co-culturing of multiple cell types. The rails work as guiding structures, and the guide rails allow fluid to flow spontaneously into the channel driven by capillary forces. This patterning mechanism requires hydrophilic circumstances. Thus, when the liquid comes into contact with the hydrophilic surface of the device, capillary forces are produced. The mechanisms of hydrogel patterning are described in more detail in our previous research. (Fig. 8) Since the rails have different heights, the first patterning of liquid only filled the central channel of the device, and the second patterning for the side channels was performed after the hydrogel in the first channel underwent polymerization. Our platform follows the standard 384-well plate format, which allows the platform to be compatible with most laboratory equipment. This implies a high availability of our device for users without any additional cost. More details are described in our previous research.

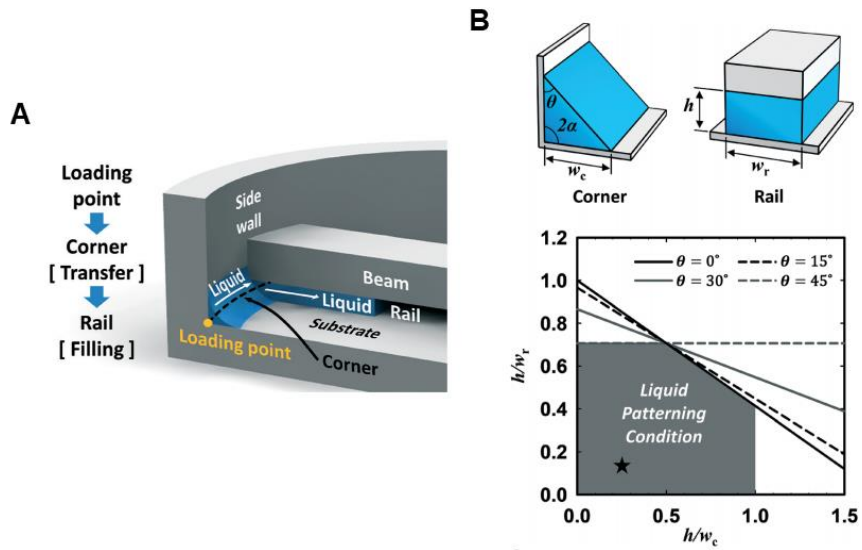


Figure 7. Principle of liquid patterning in rails. (A) The channel filled with liquid by surface hydrophilicity and capillary force. (B) According to the ratio of width and height dependent liquid patterning

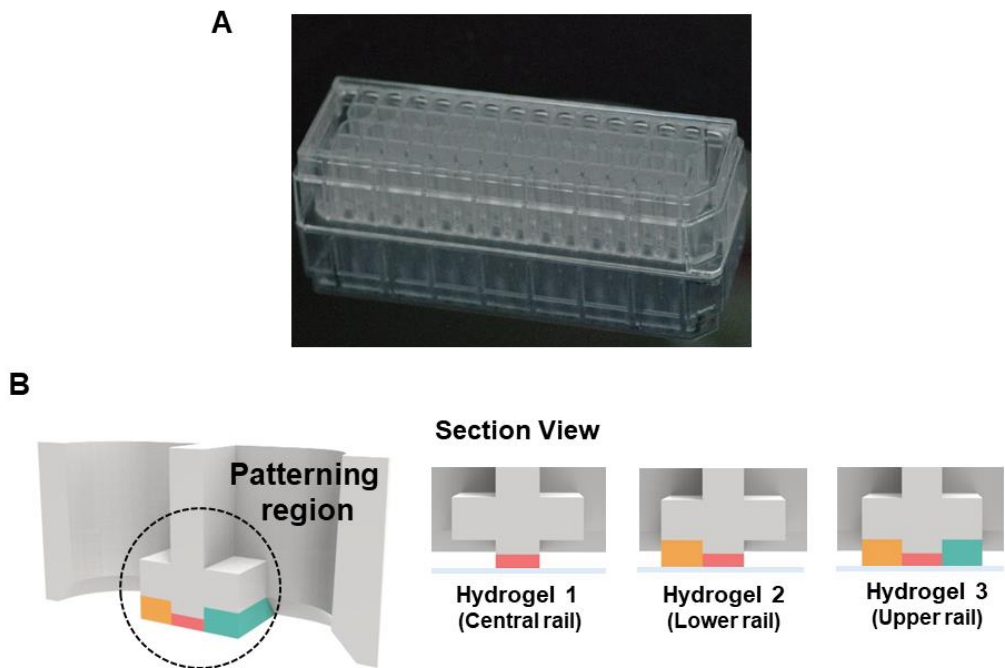


Figure 8. (A) Actual image of injection molded standard 384-well plate format microfluidic chip. The device is made of polystyrene(PS) (B) Illustration of section view and hydrogel patterning. Microfluidic device is composed of 3 parallel fluid guide rails. Fluid patterning was performed by capillary forces. Spontaneous fluid patterning was achieved by capillary force and height differences from the substrate.

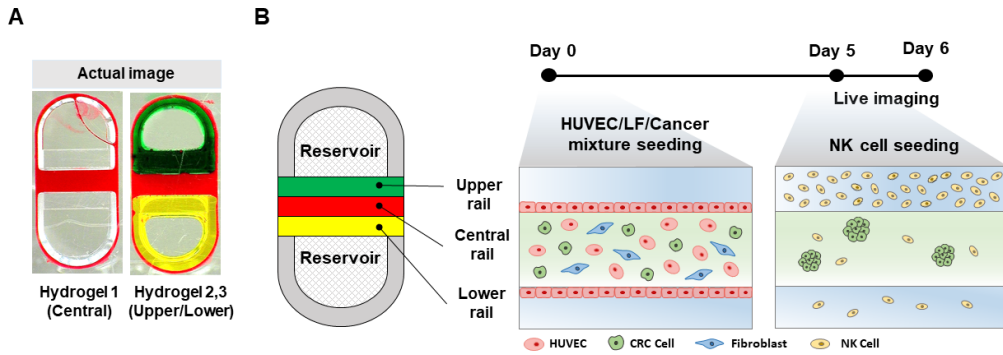


Figure 9. (A) Actual image of the channel hydrogel patterning Fill the lower microchannel with primary hydrogel. (red) Then, fill the higher micro channels with secondary hydrogel (yellow and green) respectively. (B) Experimental configuration of the microfluidic platform from cell seeding to live imaging. 5 days after cell seeding, HUVECs are fully vascularized with CRC cells. NK cells were introduced to the microvessels and the device was loaded on a live-imaging chamber.

2-3-2. Tumor vessel formation.

We examine the angiogenic sprouting(Fig 10A) and vascular formation according to stromal cell types. (Fig 10B) Without LF, no vesicular network developed and any angiogenic sprouting observed. Colon fibroblast (CF) showed similar spouting ability as LF. Cancer associated fibroblast(CAF) represent extremely fast anigiogenic sprouting. Their number of tips and length of vessels were incredibly higher than others. However, we did not used CAF in this experiment since this cell is not configured yet. Patient derived fibroblast 125T and 126T also examined. 126T showed better spouting than 125T. It is even better than those of LF. Mixture of HUVEC, LF, and CRCs with fibrin gel loaded in the central channel and formed self-assembled microvessel after 5 days. The z-stacked image was acquired on day 3 and 5 (Fig. 11A) We observed fully vascularized microvessel co-cultured with colorectal cancer. Then, we verified functional junctions of microvessel using Immunofluorescence. Platelet endothelial cell molecule was labelled with anti-CD31(orange). Tight junction Zonular occludens-1 and vascular endothelial cadherin was labelled with anti-ZO-1(green) and anti-VE-cadherin(red) respectively; We confirmed that the tight junction expression was well developed in tumor-vasculature system. (Fig 11B) Also, we confirmed the microvessel lumen formation by cross-section of 3D confocal images. (Fig. 11C)

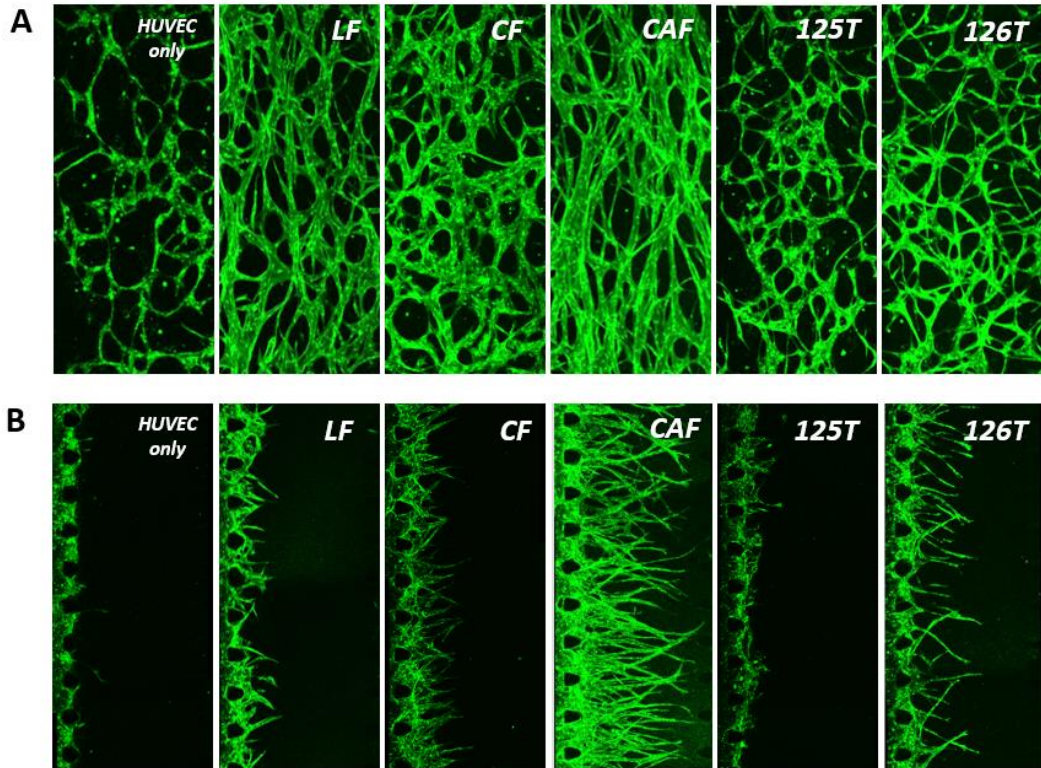


Figure 10. Stromal cell type dependent Angiogenesis and vasculogenesis (A) Angiogenesis and (B) Vasculogenesis. Cancer associated fibroblast(CAF) has great potential to vascular formation and angiogenic spouting. 125T and 126T represent patient derived fibroblast.

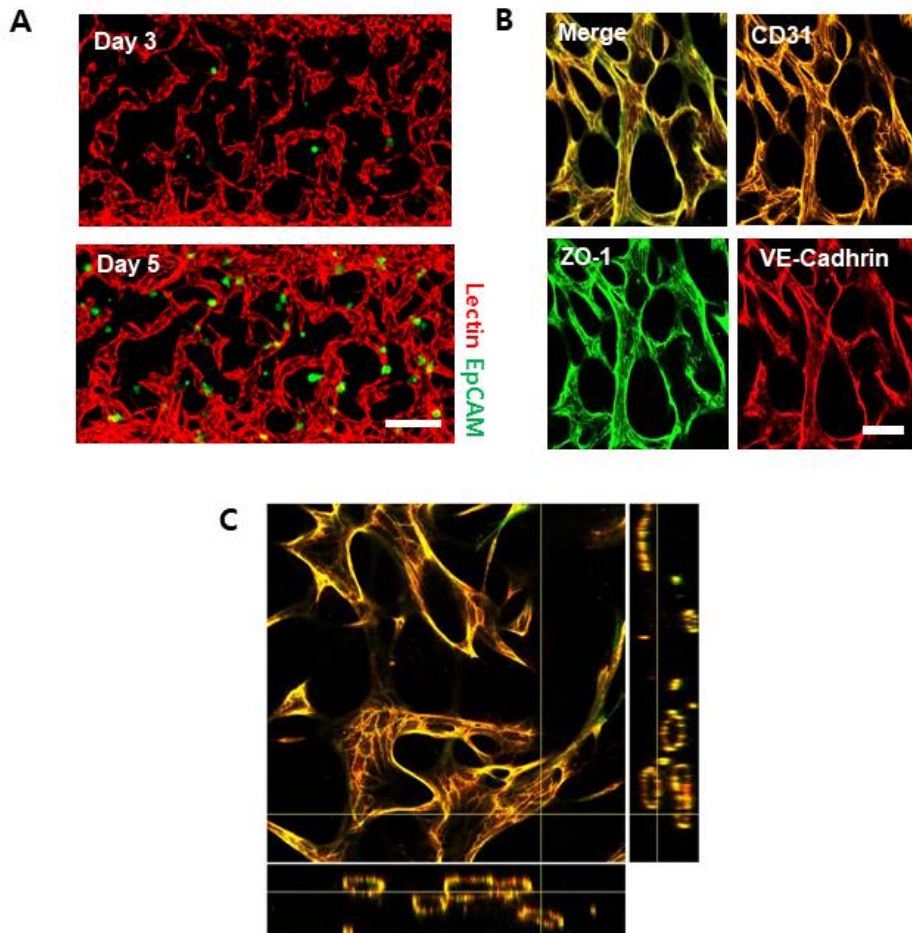


Figure 11. Confocal image of tumor vessel formation. (A) Time lapse image of tumor vessel formation. Scale bar = 100 μ m (B) Junction expression of tumor vessel. Scale bar = 100 μ m (C) Cross section image of tumor vessel to confirm lumen formation.

“

2-3-3. The effect of medium in tumor vasculature culture.

We chose 6 CRC cell lines, considering not only microsatellite stable (MSS)/microsatellite instability (MSI) subtype classification but also the consensus of molecular subtypes (CMS) classification. (Table 1) HT29, SW480, and SW620 are classified as MSS subtypes, while on the other hand, SW48, HCT116, and LoVo are classified as MSI subtypes. MSI type tumors are known to be more favorable to immune cell infiltration and anti-tumor response compared to MSS types. Recent research trends in colorectal cancer studies underline that considering CMS with distinct molecular and genomic features is more important. This categorization helps us understand immune cell infiltration and molecular immunological features of CRCs.

After seeding the mixture of cells in channel, we incubated for 5 days for vascularization. (Fig. 12) Then, we validated the optimal condition for the tumor vasculature. It is well known that the TME becomes acidic after consuming plenty of nutrients and accumulating waste such as lactate. These conditions make it difficult for ECs to be vascularized. Besides, we wanted to maximize the size of tumors located near the vessels in order to increase the probability of NK cells to migrating to CRCs by chemotaxis. Therefore, it is necessary to introduce the optimal medium condition for the sake of co-cultured tumor vasculature to compensate for nutrient consumption and eliminate acidic waste. There is one

major reason for considering the addition of extra serum to the medium. Most cancer cells are cultured in DMEM or RPMI supplemented with 10% FBS. However, EGM-2 consists of only ~2% of FBS. In the aspect of ECs, they might encounter a lack of sufficient nutrients. Therefore, we added the extra serum to satisfy both CRC cells and ECs. (Fig. 12A) As a result, the total vessel area and cancer area was increased in all CRC subtypes when the serum concentration increased up to 10%. (Fig12. B and C) SW480, SW48, HCT116, and LoVo showed increased vessel area about 7.71%, 12.85%, 10.43%, and 8.06% respectively. Under the medium condition with 10% and 20% of FBS condition, the vessels seemed abnormal (Fig 13A) and were chaotically organized, which is a major characteristic of tumor-associated blood vasculature. (Fig. 13B) On the other hand, SW480 and HCT116 showed increased total cancer area 5.03% and 4.57% for each, indicating higher proliferation rates compared to other CRC cell lines. Since a single cancer cell inside the channel proliferates and forms lumps at the end of the experiment, this result might come from not only differences in proliferation rates but also their ways to form lumps. More details will be discussed later. Additionally, the number of junctions decreased as the serum concentration increased to 10% in most of the cancers. [Fig. 12D] This structural and functional abnormality in blood vessels is the major feature in the TME. This abnormal form of vessel hinders the blood circulation especially around the tumors and obstructs drug delivery

eventually. There are several considerable features of tumor vasculature: a lack of vessels in some regions, variable vessel diameters, chaotic flow patterns, and high permeability (barrier function defection). These features are crucial in both conventional chemotherapies and the latest anti-cancer immunotherapies since they hinder target delivery. Moreover, it has been known that VEGFs released from the tumors induce angiogenesis sprouting, but recent studies conceded that the TME was noxious to microvessels. Therefore, we focused on defining the adequate condition for *in vitro* tumor vasculature as a standard model to study the TME itself and the effect of drugs or immune cells on tumors.

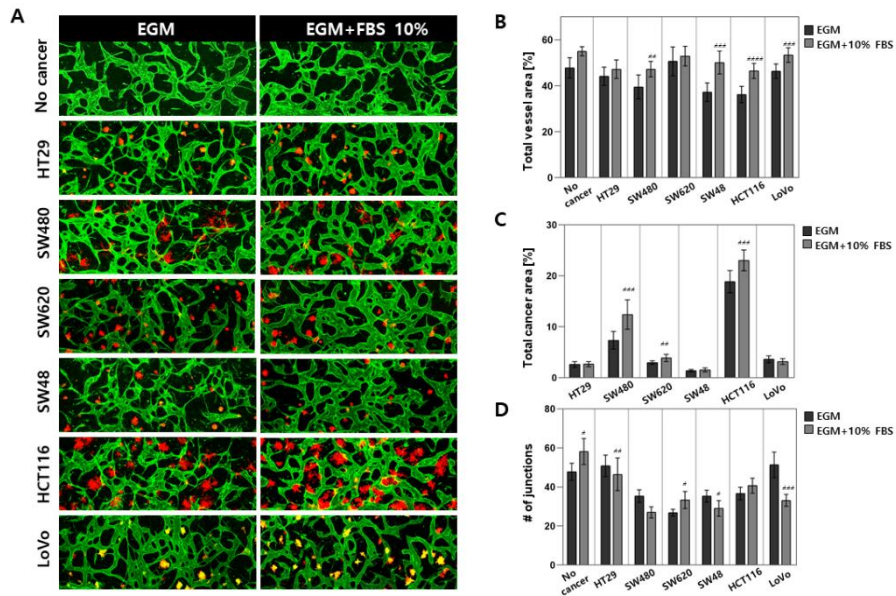


Figure 12. The effect of culture medium condition on tumor vasculature. (A) Confocal image of tumor vasculature with various CRCs according to culture medium conditions. By adding 10% FBS to EGM-2, we benefited both endothelial cells and CRCs simultaneously. Scale bar = 100 μ m (B) Total vessel area (C) Total cancer area. (C) the number of junction were measured.

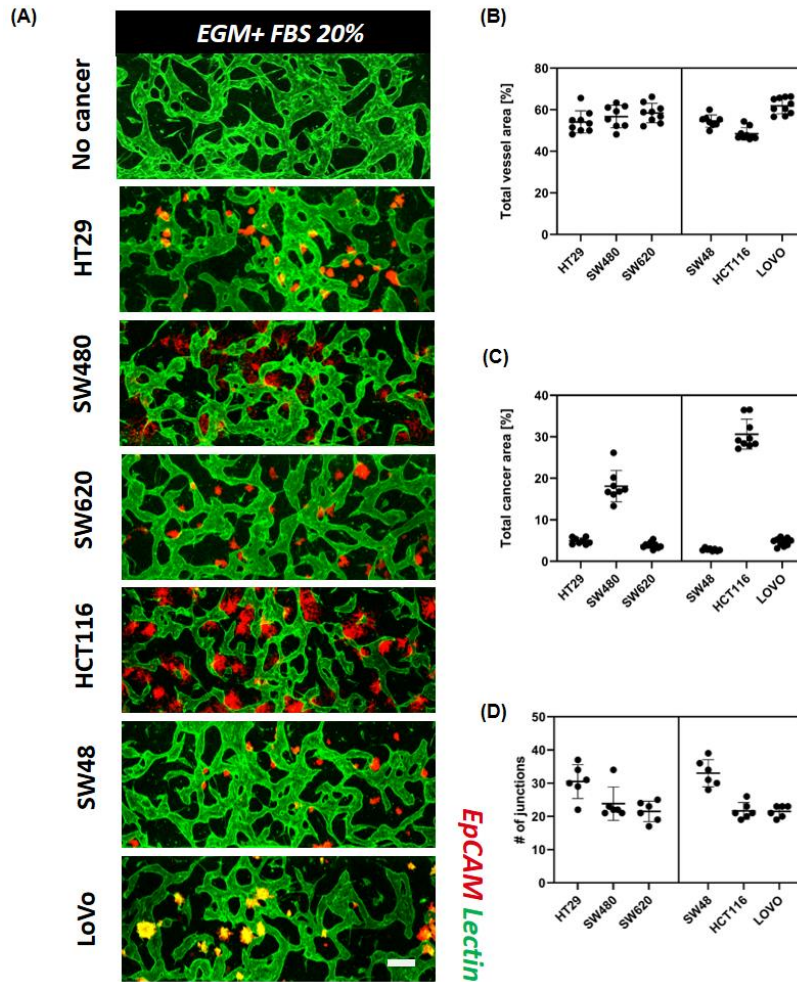


Figure 13. The effect of EGM-2 supplemented with 20% FBS on tumor vasculature. (A) Representative confocal image of tumor vessel in EGM-2 supplemented with 20% FBS. Scale bar = 100 μ m. (B) Total vessel area (B) Total cancer area (C) The number of junctions were measure.

2-3-4. CRC concentration optimization

Since CRCs produced a lot of waste and acidic byproducts such as lactic acid, we optimized cancer cell concentration in order to preserve the formation of blood vessels. We verified the cancer cell concentration ranging from 0.1 mil/mL to 0.3 mil/mL due to the high proliferation rate of cancer cells. [Fig. 14A] We used an EGM-2 medium supplemented with 10% FBS. As a result, there was little difference in the total vessel area when the cancer cell concentration increased from 0.1mil/ml to 0.2 mil/ml.

Only HT29 and HCT116 showed increased vessels under the 0.2 mi/ml condition about 7.39% and 9.22% respectively. On the other hand, the total vessel area decreased in most cell types when the cancer cell concentration was at 0.3mil/ml (Fig. 11B) In HCT116, we measured total vessel length and the number of junctions, however, no significant result observed. (Fig. 15) Especially, SW480 and HCT116 showed about 4.69% and 10.48% decreases in the total vessel area. We assume that this result represents the pro-angiogenic effect of CRCs and the effect of acidic waste on blood vessels. We concluded that some factors and cytokines such as VEGF-A released from tumors enhanced angiogenic sprouting until the effect of waste from the tumors overwhelmed. In other words, the effect of pro-angiogenic factors was dominant up to a certain point, and thereafter the effect of waste secreted from cancer cells prevailed. Therefore, we reached a decision to use

0.2 ml/ml of cancer cell concentration to maximize the cancer size while the microvessels are kept thoroughly.

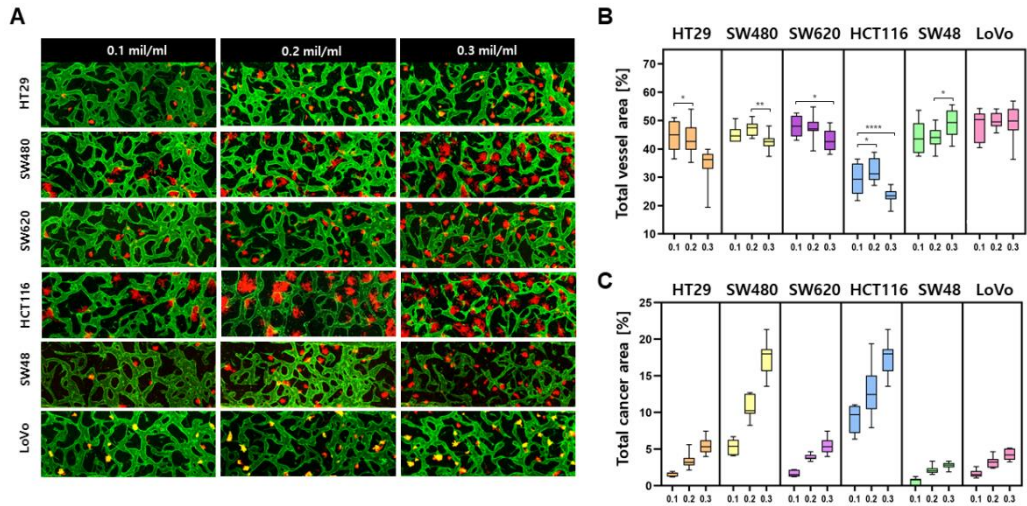


Figure 14. The effect of CRC concentration for tumor vasculature. (A) 3D confocal image of microvessels (lectin, green) with various CRCs (EpCAM, red) according to the CRC concentration. (B) Total vessel area decreased when the cell concentration of 0.3mil/ml of CRC was loaded. CRC concentration of 0.2 mil/ml is the optimal condition for both microvessels and cancers. (C) Total cancer area according to the CRC concentration. Each cell proliferates at a different rate and size.

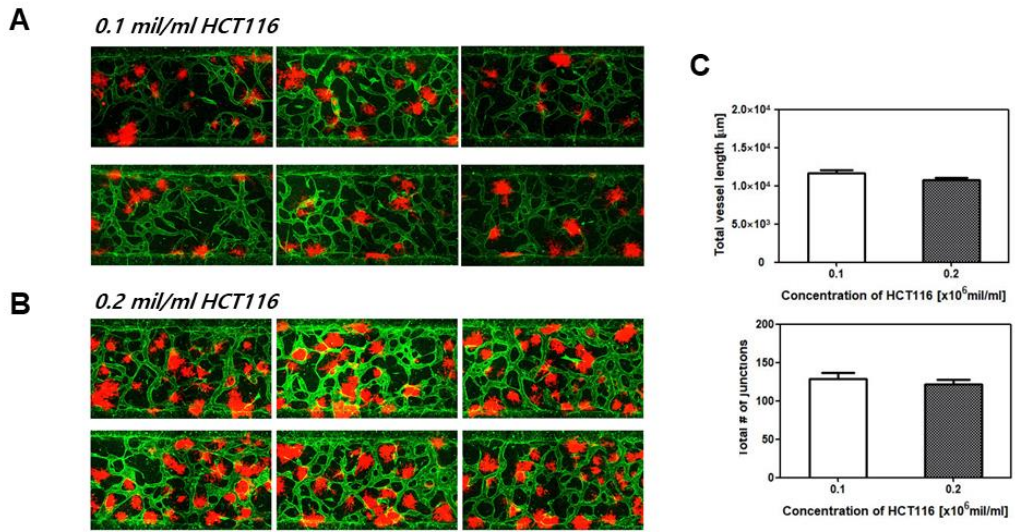


Figure 15. The effect of HCT 116 cell concentration on tumor vasculature. (A) Confocal image of tumor vessel in condition of 0.1 ml/ml of HCT116. (B) Confocal image of tumor vessel in condition of 0.2 ml/ml of HCT116. (C) Total vessel length and total number of junction were measured. Not significant result observed.

2-3-5. The characteristics of tumor vasculature

CRCs co-cultured with HUVEC formed different morphologies of tumors at day 5 after seeding. CRCs were mixed with other cells such as LFs and HUVECs at the beginning of the experiment. They proliferated and formed peculiar lump shapes. The shape of cancerous lump varies from the spherical to star-like shapes, depending on the types of CRCs. We focused on the individual lump size since we assumed that the larger the cancer size, the more chances there would be for lymphocytes to extravasate from the vessels and kill cancer cells. As a result, HT29, SW620 and SW48 formed the smallest lumps and the shape of the lump was close to a spherical shape. (Fig. 16A) Even though the FBS concentration increased up to 20%, there were no significant differences in individual cancerous lumps size distributions. (Figure 16B) On the other hand, HCT116 and SW480 formed wide and sparse star-shaped lumps. (Fig. 13A and B) Since the size of the lumps is larger than other CRC cell lines, we expected more lymphocytes to extravasate from blood vessels to the tumor site. Moreover, the individual cancerous lump size varies in all medium conditions.

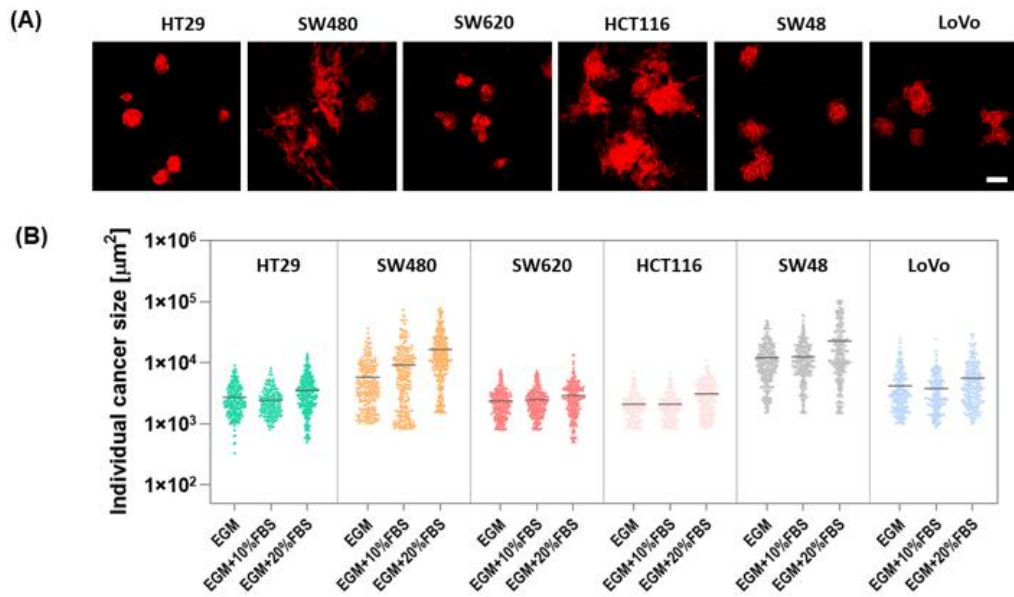


Figure 16. Morphological differences and size distribution of CRC cells. (A) CRC cells formed different shape of lumps in tumor vessel microenvironment. (B) Size distribution of CRC cells.

In addition, we evaluated the vessel permeability coefficient when co-cultured with various CRCs. Microvessel permeability measurements were performed on day 5. Fully vascularized perfusable microvessels were labelled with lectin (red) and EpCAM (green). Before taking measurements, each reservoir was emptied and filled with a solution containing fluorescence dye. Cascade blue (MW=3kD) was used to measure the endothelial barrier permeability. The device was imaged every 20 s for 10 min inside the live-cell imaging chamber. Figures 17A and B show time series confocal images of microvessels, and fluorescence dye (blue) was utilized for analyzing intensity changes in perivascular regions to measure the permeability. The perivascular region around the vessel showed a slight increase in fluorescence intensity due to the fluorescence dye that passed through the blood vessel barrier. Permeability coefficient P was calculated based on the equation below:

$$P = \frac{1}{l_w} X \frac{dl/dt}{I_j}$$

where l_w is length of the vessel wall that separates the perivascular and microvessel regions, I_j is the mean intensity in the microvessel region, and I is the total intensity in the perivascular region. A more detailed derivation of this equation is described in our previous research. As a result, the microvessels co-cultured with cancers became leaky compared to normal microvessels, confirming a significant feature of tumor vasculature. (Fig 15) Fluorescence dye started to leak

from the weak part of the microvessel, marked by a dashed white circle. Figure 18 shows a relative permeability coefficient induced by different colorectal CRC types. The vessels induced by HT29 and SW480 show significantly higher permeability compared to the vessels without cancer cells.

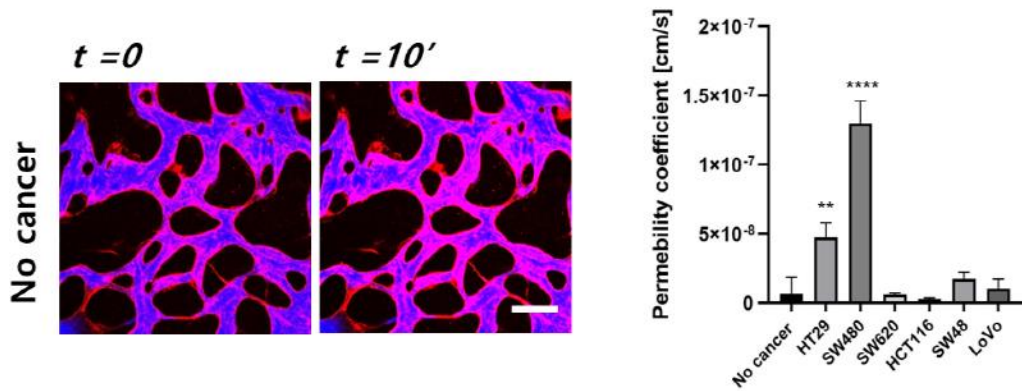


Figure 17. Permeability measurement of normal and tumor vasculature. (A) Time-lapse 3D confocal image of normal vasculature. Microvessels and colorectal cancers were labelled with lectin (red) and EpCAM (green) respectively. Cascade blue (MW=3kD) was used to measure vascular permeability. Scale bar = $50\mu\text{m}$ (B) Relative permeability coefficient of tumor vasculature. HT29 and SW480 showed relatively higher permeability coefficient.

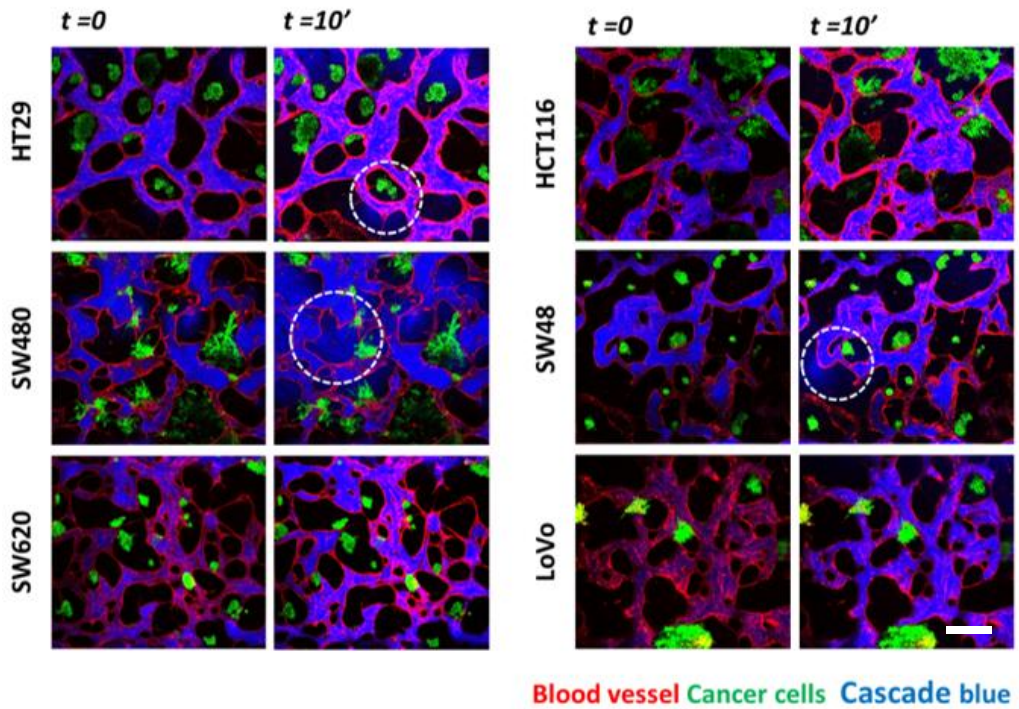


Figure 18. Permeability measurement tumor vasculature. (A) Time-lapse 3D confocal images of tumor vasculature. Microvessels were relatively leaky compared to the normal vasculature. Fluorescence dye leaked from the weak part of the microvessel marked by a white dashed circle. Microvessels and colorectal cancers were labelled with lectin (red) and EpCAM (green) respectively. Cascade blue (MW=3kD) was used to measure vascular permeability. Scale bar = 50 μ m

2-3-6. Validation of NK cell cytotoxicity in 3D complex TME

Using our model, we demonstrated NK cell cytotoxicity assays according to the types of CRCs. Since lymphocytes such as NK cells, T cells and dendritic cells are circulating the blood vessels and monitoring the tumor as a part of immune surveillance, the validation of their cytotoxicity should be performed in the complex 3D TME. We compared the cytotoxicity of NK cells on a conventional 2D cell culture dish as well as our 3D culture platform. Cancer cells and NK cells were labelled with EpCAM (green) and CellTrace (orange). Dead cancer cells and dead NK cells were labelled with PI (red) and SYTOX (blue). As a result, most of the cancer cells were dead 4 hours after NK cell loading on the 2D culture dish, (Fig. 16) while NK cells in our complex 3D tumor vasculature platform showed relatively slower cytotoxic activity compared to the 2D culture platform. (Fi. 19) NK cells underwent extravasation and intravasation through the microvessels. (Fig.17A and C) They extravasated toward the tumor sites (Fig. 20A) and killed CRC cells. SYTOX blue signal appeared right after the attacks by NK cells, representing the dead cells. It took roughly 3 and a half hours from extravasation to intravasation. Intriguingly, among the number of NK cells that extravasated the microvessel, not all the cells were involved in the cytotoxic activity.(Fig 20C) Only a few NK cells attacked the cancer cells, resulting in the cytotoxic effect and low viability in cancer cells. We also validated the NK cytotoxicity according to the

CRC types. NK cells showed distinct cytotoxic activity according to CRC CMS types. CMS classification classifies CRCs into 4 molecular subtypes with distinct biological characteristics. CMS1 type CRCs are called “immune activated” and these recruit a number of intratumoral immune cells which are usually in an active state.

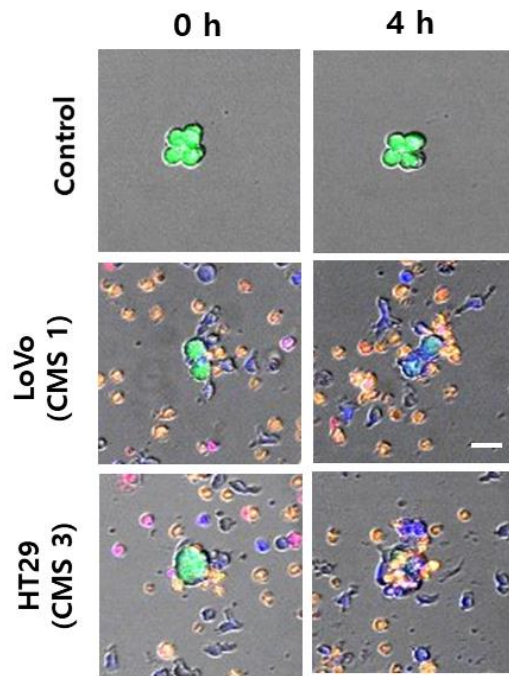


Figure 19. Cytotoxic activity of NK cells on a 2D culture dish. Live CRC (green), dead CRC (Blue), live NK cells (white) and dead NK cells (red) were labelled with EpCAM, SYTOX Blue, CellTrace Far Red, and PI. (Scale bar = 10 μ m)

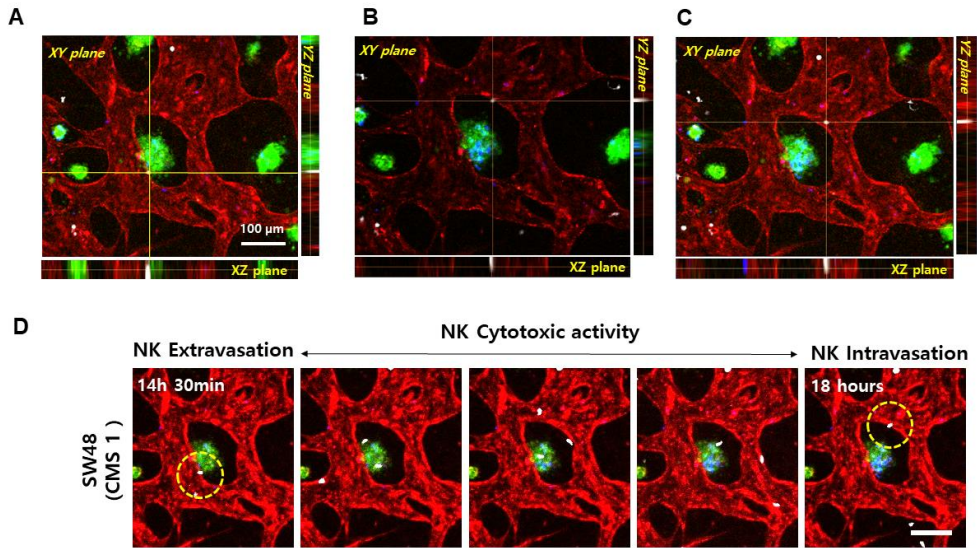


Figure 20. 3D confocal image of NK cytotoxicity and infiltration in 3D tumor vasculature. (A) Cross section of NK cell extravasation. (B) intravasation (C) after intravasation. Blood vessel (red), live CRC (green), dead CRC (blue), and NK cells (white) were labelled with lectin, EpCAM, SYTOX blue, and CellTrace Far Red, respectively. (D) Time lapse imaging of NK cell extravasation, cytotoxic activity and intravasation. Live imaging was performed for 24 hours.

On the other hand, CMS 3 type CRC cells are called “immune excluded” and have some intratumoral immune cells. (Fig. 23) [Emilie Picard et al., *Front. Immunol.*, 2020] We examined 6 different CRC cells containing CMS 1, 3, and 4. As a result, NK cells showed much higher cytotoxic activity against CMS 1 type cancer cells compared to other types. (Fig. 21A) SW48 and LoVo were used to represent CMS 1 type CRC, HT29 was used to represent CMS 3 type CRC, and SW480, SW620, and HCT116 were used to represent CMS 4 type CRC. There have been no significant differences between CMS 3 and 4 type CRCs. NK cells showed higher cytotoxicity against only SW48 and LoVo, while SW620 also slightly induced the NK cell cytotoxicity; however, a notable result has not been found. (Fig. 21B) We also quantified the number of NK cells extravasated and the death rate of CRCs during the time-lapse live cell imaging. As a result, HT29 showed lower number of NK cells extravasated and death rate compared to SW48 cells. This result implies that other types of CRCs except CMS1 induced not only the lower cytotoxic activity of NK cells but also lower number of intratumoral NK cells extravasated. (Fig. 22) In addition, we verified NK cell cytotoxicity according to their population. We used 0.05 mil/ml and 0.1 mil/ml of NK cells. Under the 0.05 mil/ml condition, LoVo was killed after 22 hours. (Fig. 20) On the other hand, NK cells spent only 10 hours to kill LoVo under 0.1 mil/ml conditions. (Fig. 23) Consequently, NK cells with high densities represent faster cytotoxic

activity to cancer cells. Meanwhile, there has been no cytotoxic activity observed in HT 29 in both conditions. These results confirmed again that our platform is clinically meaningful and can be used as a potential substitute for conventional cancer research platforms.

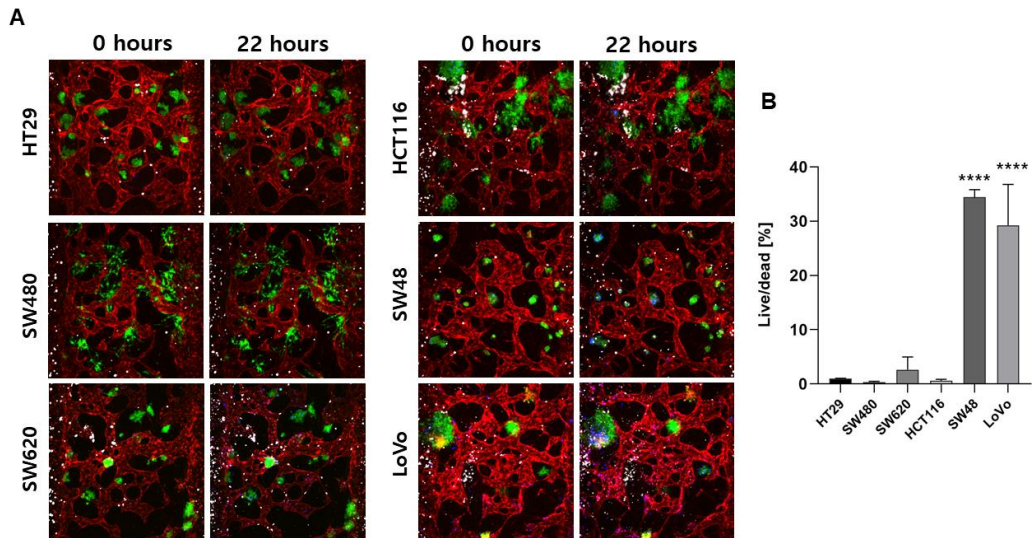


Figure 21. 3D confocal image of NK cytotoxicity to various CRC cells. (A) Confocal image of NK cytotoxic activity. (B) Quantification of CRC cells viability after NK cytotoxic activity.

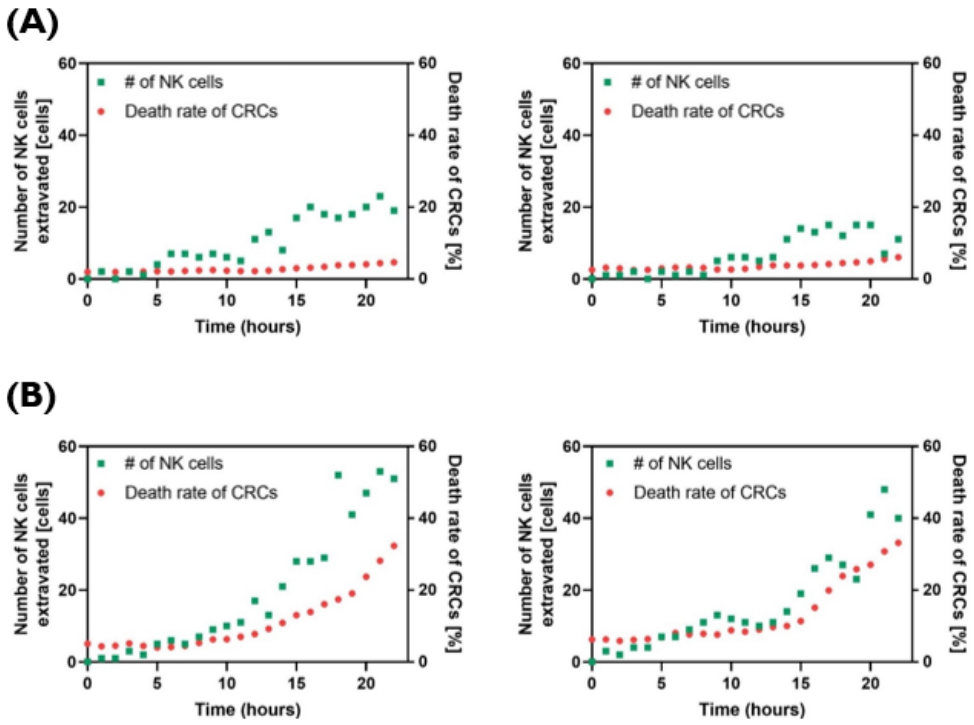


Figure 22. Number of NK cells extravasated and death rate of both (A) HT29 and (B) SW480 during live-cell imaging. SW48 cells showed the higher number of NK cells extravasated and death rate.

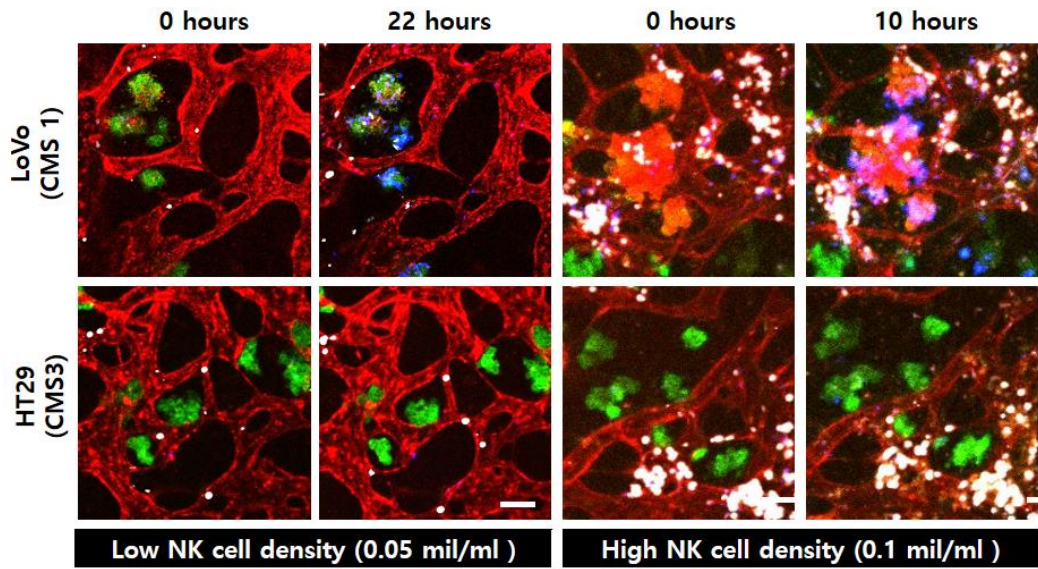


Figure 23. The effect of NK cell number on cytotoxic activity. NK cell showed faster and higher cytotoxic activity to LoVo, which is classified to CMS 1. Scale bar = 100 μ m

2-4. Summary

We developed an injection-molded microfluidic platform that can reconstitute a tumor vasculature as well as key components in the CRC TME. The platform that comprised 28 wells with the standard 384-well plate format allowed us to perform high throughput experiments and provided an effective method of defining the optimum cell culture conditions for perfusable blood vessels co-cultured with CRC cell lines. Morphological and functional differences including permeability between tumor and normal vasculatures on the platform showed that we constructed the physiologically relevant tumor vasculature with its aberrant structures and higher permeability. After perfusable blood vessels were formed, NK cells were introduced into the vessels for the validation of cytotoxicity assays against different CMS subtypes of CRC cell lines. Intriguingly, the highest cytotoxic activity of NK cells could be observed in LoVo and SW48, which have CMS 1 subtype. Our platform has a wide range of potential applications, from studying immune-cancer cell interplays in the TME to drug screening for chemotherapy and immunotherapy.

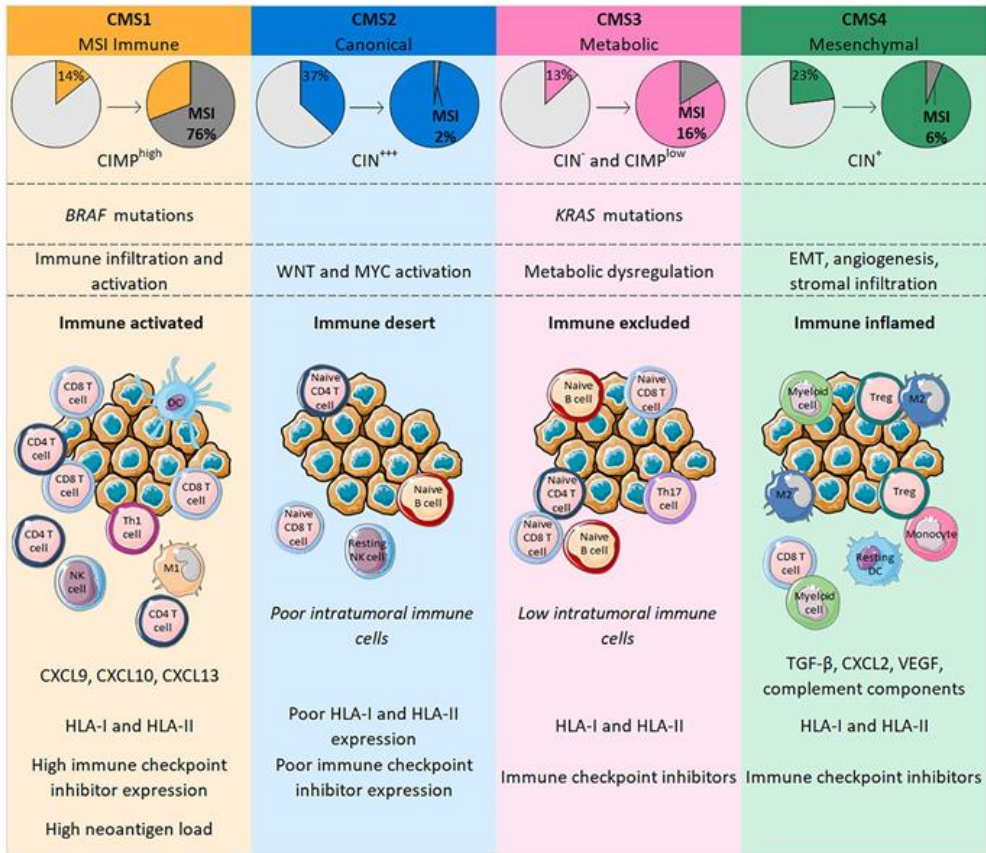


Figure 24. CMS in CRC are classified according to genetic modifications and intratumoral immune phenotype, with distinct profiles. CMS1 tumors are enriched with activated immune cells.

Chapter 3

The effect of tumor-associated macrophage(TAM) on Colorectal cancer and tumor microenvironment.

3-1. Introduction

Colorectal cancer (CRC) is the second leading cause of cancer-related death. As cancer-immunotherapy is opening a new paradigm for cancer therapy, there have been many researches to elucidate correlation between cancer and inflammatory cells such as monocyte, T cells and natural killer cells. As several recent study reported TAM leads to a favorable prognosis on CRC, TAM is becoming one of promising candidate in tumor progression. TAM displays opposite behavior depending on their polarization. M1(classically activated) phenotype in to secrete pro-inflammatory cytokines, while M2(alternatively activated) phenotypes in to secrete anti-inflammatory cytokines. Therefore, M1 macrophage inhibit the tumor progression whereas M2 macrophage enhance.

As so far, these studies have been performed in conventional 2D cell culture system *in vitro*. However, 2D cell culture system rarely reflect complex 3D cellular microenvironment. Recent advances in microfluidic techniques have enable researchers to mimic physiologically relevant engineered tumor micro environment

(TME) over 2D cell culture. For instance, there have been several researches to elucidate monocyte infiltration through the endothelial barrier. In aspect of complex 3D tumor microenvironment accompanied with perfusable blood vessel, there are still absence of complete model system. (Fig. 25) Especially, CRCs are highly metastatic to liver via portal vein and decreased the five-year survival rate to 11% consequently. Therefore, it is essential to consider blood vessel to study colorectal cancer *in vitro*.

We recently reported open microfluidic based injection molded plastic chip, which is composed of 3 parallel rails. These rails enable us to pattern hydrogel with different cell types. In addition, we optimized the co-culture condition for colorectal cancers with micro vessel. Perfusable characteristics observed in central blood vessel, enabling us not only anti-cancer drugs screening but also a validation of the immune cells infiltration.

Here is the major reason we used conditioned medium instead of introducing macrophage itself. In a manner of attack tumors, macrophages release cytokines rather than physically contact to cancer cells. For instance, natural killer cell, CD4+ T cells, and CD8+ T cells physically bind to cancer cells for cytotoxic activity. Meanwhile, macrophage does not. Therefore, we validate the effect of M1 and M2 macrophage on colon cancer cells and their microenvironment by using CM from each macrophage.

	Park <i>et al.</i>	Li <i>et al.</i>	Lee <i>et al.</i>	Kim <i>et al.</i>
Device Schematics				
Representative result				

Figure 25. Previous study of immune cells in microfluidics.

3-2. Materials and Methods

3-2-1. Cell culture

Human umbilical vein endothelial cells (HUVECs, Lonza) were cultured in endothelial growth medium (EGM-2) with supplements. Normal human lung fibroblasts (LFs, Lonza) were cultured in fibroblast growth medium (FGM-2, Lonza) and passage 6 was used for the experiments. The human colon cancer cell line LoVo, SW480, and human monocyte cell line THP-1 were culture in RPMI 1640 supplemented with 10% Fatal bovine serum(FBS). All cells were cultured in a humidified incubator at 37 °C and 5% CO₂.

3-2-2. Condition medium (CM) preparation

To polarize into M0 macrophages, THP-1 cells were prepared at a concentration of 1×10^7 and stimulated with 320 nM phorbol 12-myristate 13-acetate (PMA) for 24 hours. To polarize into M1 or M2 macrophages, THP-1 cells were PMA-treated for 6 hours, with addition of M1-polarizing reagents [100 ng/ml lipopolysaccharide plus 20 ng/ml interferon gamma] or M2-polarizing reagents [20 ng/ml IL-4 plus 20 ng/ml IL-13] during the final 18 hours, respectively. After macophage polarization, the culture supernatants were collected as M0 CM, M1 CM or M2 CM and stored at 4°C.

3-2-3. Live/dead assay for HUVECs

HUVEC suspension at a concentration of 1×10^6 cell per ml were mixed with fibrinogen solution (2.5 mg/ml with 0.15 U/ml aprotinin) at 3:1 ratio. 0.9 μ l of this mixture was loaded to central channel. Various concentration of CM was prepared by serial dilution with EGM. Diluted CM was introduced to medium reservoir. Samples were stained with calcein-AM/ethidium homodimer-1 kit and imaged every 4h, 8h and 12 h.

3-2-4. Design and fabrication of chip

The plastic chip was designed by using solidworks. The device consists of 3 parallel channels enabling co-culture of different cell types, respectively. Liquid go through the guide rail by capillary force. Polystyrene(PS) was used for injection molding at an R&D Factory (Korea). The aluminum alloy was fabricated by machining and polishing. The clamping force of mold was set at 55 bar with injection pressure of 55 bar, 15 seconds pf cycle time and a 220°C nozzle temperature. The thin film was used as a substrate of device and bonded to chip by simply pressing.

3-2-5. tumor-vasculature formation

HUVEC/LF/CRCs suspensions were prepared at a concentration of 12 mil/ml, 8 mil/ml and 2mil/ml respectively. The cell suspensions were mixed with 10mg/ml fibrin gel. Therefore, the final concentration of HUVEC/LF/CRCs were 6mil/ml, 2mil/ml and 0.2 mil/ml. The 0.9 μ l of mixture was introduced to central channel. After gelation, each reservoir was filled with 100 μ l of EGM-2 supplemented with extra 10% FBS. The medium changed every day. The cells were cultured for 5 days to fully vascularized.

3-2-6. Immunofluorescence assay

All medium in each well was removed before fixing. Samples were fixed using 4% paraformaldehyde (Biosesang) for 15 min and 0.2% triton-X 100(Sigma-Aldrich) for 20 min subsequently at room temperature. 3% bovine serum albumin (BSA, Sigma) solution in PBS was used to block non-specific bonding of antibodies. Alexa Fluor® 488 anti-human CD54 Antibody and Alexa Fluor® 594 anti-human CD144 (VE-Cadherin) Antibody were purchased from Biolegend. Phospho-VE-cadherin (Tyr658) Antibody and Goat Anti-Rabbit IgG H&L Alexa Fluor® 594, secondary antibody was used to labelled VE-cadherin and phosphor-VE-cadherin, respectively. (Thermofisher) All the antibodies were diluted with BSA solution described above according to enclosed instruction. All of the samples were stored

at 4°C for overnight, and then washed with PBS until imaging.

3-2-7. Live/dead assay for CRCs

CRC suspension at a concentration of 0.5×10^6 cell per ml were mixed with fibrinogen solution (2.5 mg/ml with 0.15 U/ml aprotinin) at 3:1 ratio. 0.9 µl of this mixture was loaded to central channel. Then, the device was incubated for 5 min for gelation and Reservoirs were filled with CM. The samples were incubated for 8 hours. After incubation, the samples were stained with Calcein-AM/ethidium homodimer-1 kit and incubated again for 30 min. Fluorescence image was obtained by using confocal microscope.

3-2-8. Quantification of tumor proliferation

To synchronize the cell cycle, a culture dish was washed with PBS several times and filled with RPMI without serum for 12 hours. Cell preparation and hydrogel loading method was same with live/dead assay described above. After the introducing cells to the device, each reservoir was filled with CM and incubated for 12 hours. Samples were fixed and stained with ki-67 marker and Hoechst as described below.

3-2-9. Preparation for Fibrin Gels for Scanning Electron Microscopy

To prepare for the fibrin gels, 2.5 mg/ ml bovine fibrinogen (Sigma) was dissolved

in PBS (Gibco) and aprotinin (0.15 U/ml, Sigma) supplemented in the solution. For the cell-suspended fibrin gels, SW480, HUVECs, and LFs were suspended in the fibrinogen solutions, at a concentration of 0.2×10^6 cells ml⁻¹ for SW480 cells, 6×10^6 cells ml⁻¹ for HUVECs, and 3×10^6 cells ml⁻¹ for LFs. 200 μ L of the solutions were mixed with thrombin (0.5 U ml⁻¹, Sigma) and then loaded in a 48-well plate (ThermoFisher). The cell-suspended fibrin gels and acellular fibrin gels were allowed to crosslink for 5 min before the wells were filled with EGM-2. After clotting the gels and loading EGM-2 in the wells, the 48-well plate was incubated at 37 °C in 5% CO₂ for 4 days. After 4 day-incubation, the medium in each well was removed, and each well was filled with EGM-2, M0, M1, and M2 (each media), respectively. The well plate was incubated at 37 °C in 5% CO₂ for 24 h.

3-2-10. Fixation and Dehydration of Fibrin Gels for Scanning Electron Microscopy

The field emission scanning electron microscopy (FE-SEM) was used to observe the microstructure of fibrin gels. SEM investigation of the microstructure was conducted through critical point drying and platinum coating of samples. The constructs were washed in PBS, then fixed in a 2% glutaraldehyde solution for 2h. And the constructs were washed in 0.05 M sodium cacodylate buffer for 10 min, and the washing step was repeated washing step is repeated twice. Fixation was

followed with 1% osmium tetroxide for 1 h at 4 °C. Then, fixed samples were dehydrated through a series in 30, 50, 70, 80, 90, 100 (× 3) ethanol solutions for 10 min each. Subsequently, dehydrated samples were placed in a critical point dryer (Leica EM CP300, Germany), and ethanol was replaced with CO₂ and removed. The dried samples were mounted on aluminum stubs, sputter-coated with platinum, and examined by FE-SEM (S-5000, Hitachi).

3-2-11. Fluorescence Imaging and analysis

Time-lapse fluorescence imaging was acquired using an inverted fluorescence microscope system (Nikon Ti-3 Eclipse) with external shutter changer (Lambda 10-3 Sutter). 3-dimensional fluorescence image was acquired using a confocal microscope system (Nikon Ti-1 A1). NIS-elements was used as imaging software. Obtained images were analyzed using Image-J.

3-2-12. Cytokine assay

The device with vascularized tumor was prepared as described above. Medium in reservoir was aspirated and replaced with CM diluted with EGM at 1:1 ratio. After 8h, the supernatants were collected and analyzed by human cytokine array kit (Cat#. ARY005) was purchased by R&D SYSTEMS. X-ray was exposed.

3-2-13. Permeability coefficient measurement

Specially designed PDMS device was used to measure accurate vessel permeability. By limiting the diffusion direction to one side, measuring of accurate vessel permeability was achieved. More details about device is described our previous research. LF and CRC suspensions were prepared at a concentration of 8×10^6 cells/ml and mixed at 10:1 ratio. This mixture was loaded into LF channel, and HUVEC suspension at a concentration of 7×10^6 cells/ml was loaded in to medium channel. The device was tilted 90° in an incubator for 40 min to attach the cells to the fibrinogen gel surface. The device was incubated for 10 days to form fully lumenized microvessel. Then, FITC-dextran (10Kd, Sigma) was loaded into medium channel and imaged every 15 s for 5 min using inverted fluorescence microscope (Nikon, Ti-e eclipse) with 20x objective.

3-2-14. Statistical analysis

Using Prism (GraphPad, USA) was used as statistical comparisons of the values. These analysis was obtained from an unpaired two-tailed Student's t-test analysis, with the threshold for statistical significance set at * $p < 0.1$. ** $p < 0.01$; *** $p < 0.001$; **** $p < 0.0001$; and ns (not significant). Error bar is presenting the standard error of the mean.

3-3. Result and Discussion

3-3-1. The effect of Macrophage CM on colorectal cancer

Before we validate the different effect of condition medium on colorectal cancer, we confirmed the functional feature of our tumor-vasculature model. Then, we tried to validate the effect of 2 different types of macrophage not only on colon cancer cell itself but also in the 3D tumor-vasculature model. Unlike T or natural killer cell, macrophage attack tumor by secreting cytokines rather than directly contact tumor. Therefore, we used CM instead of introducing monocyte/macrophage directly to blood vessel. M0, M1 and M2 macrophages were characterized by CXCL9 and CD23 marker (Fig. 26A) and they showed different morphologic feature for each types. M1 macrophage showed elongated shapes while M2 macrophages showed round shape similar to M0. However, the size of M2 macrophages was smaller than that of the M0 macrophages (Fig. 26B). Next, we validate the cell viability and proliferation rate according each macrophage phenotype, after introducing CM to colon cancer cells. Studies have reported that microsatellite stability (MSI) status was associated with clinicopathological features of CRC patients. Hence, to validate the effect of macrophage CM on colon cancer cells according to MSI status, SW480 (MSS) and LoVo (MSI) cells were used. Colorectal cancer viability under CM was validated by immunostaining assay

using EthD-1/Calcein AM (Fig. 27C). M1 CM induced dramatic apoptosis on tumor cells while M2 CM inhibited cell death in compared to M0 CM. However, there have been no significant differences between MSI status. Furthermore, we found that cleaved form of Caspase3 and PARP, which are both mediators of programmed cell death, were remarkably increased in M1 CM treatment (Fig. 26B). The death rate of SW480 under M1 CM was about 47%, which is higher than that of M0 or M2 CM condition. The death rate of SW480 under M0 and M2 CM was about 4% and 8%. Likewise, the death rate of LoVo under M0, M1 and M2 CM condition was 20%, 61% and 8%, respectively. LoVo showed slightly higher death rate under M0 CM compared to that of SW480 (Fig. 27C). In the meantime, we validate proliferation rates using Ki-67 marker which widely used as a proliferation marker especially in human tumors. (Fig 25A) The proliferation rates showed opposite results. M1 CM treatment clearly decreased the viability of SW480 and LoVo cells while M2 CM increased the Ki-67 expression of these colon cancer cells compared with M0 CM condition (Fig. 27D). These result confirmed again that M2 macropahges are pro-tumorigenic by inducing cancer cell proliferation and M1 macrophage are anti-tumorigenic by inducing apoptosis dependent cell death.

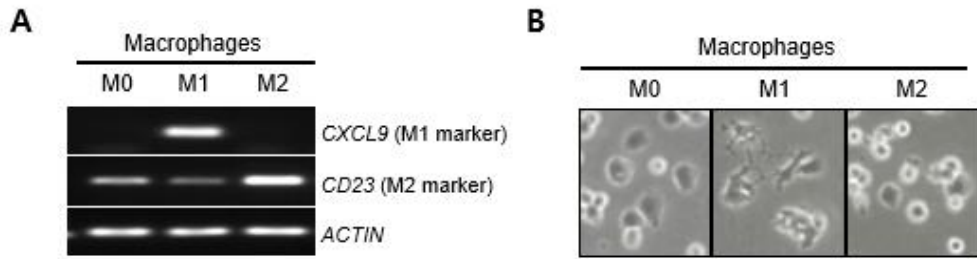


Figure 26. Macrophage differentiation. (A) Macrophages were differentiated in to M0, M1, M2 respectively. We confirmed with M1(*CXCL9*) and M2 marker(*CD23*). (B) Photograph of differentiated macrophage.

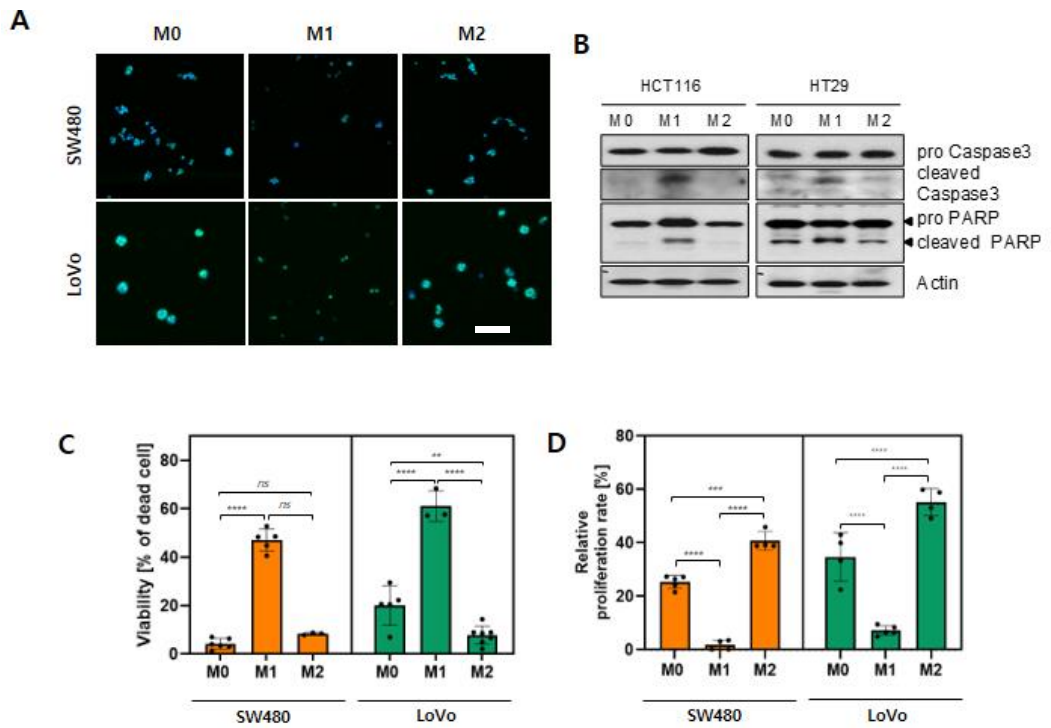


Figure 27. The effect of macrophage on CRC cells (A) Ki-67 expression in SW480 and LoVo. Scale bar = 30 μ m (B) Western blot of Caspase and PARP (C) Viability of CRC cells (D) Relative proliferation of CRC cells.

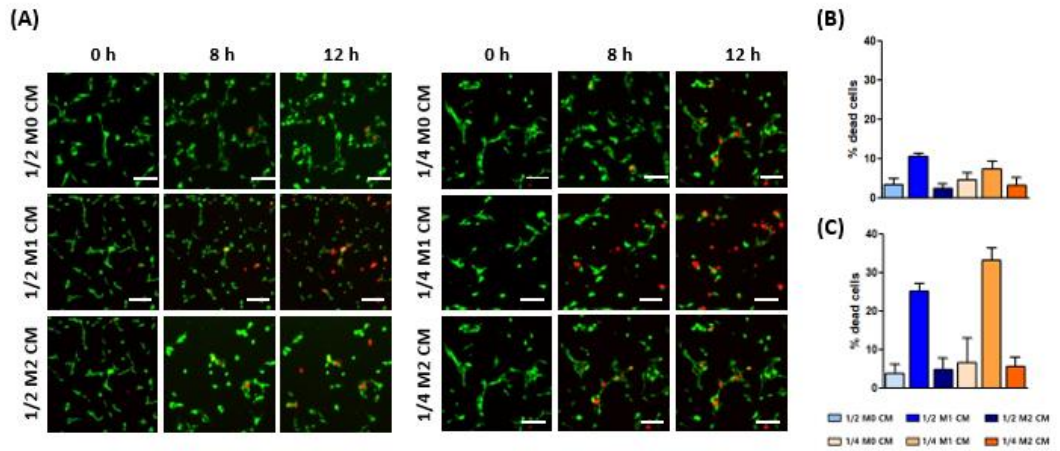


Figure 28. The effect of macrophage on HUVEC. (A) Confocal image of HUVEC Live/dead image under various concentration of CM. (B) Measurement of viability of HUVEC according to CM concentration.

3-3-2. The effect of macrophage on tumor microenvironment (TME)

Since macrophage involves not only tumor progression but also angiogenic process and extracellular matrix(ECM) remodeling, we tried to reconstruct the effect of macrophage according to their phenotype on TME. We simply observed the effect of CM on ECM by SEM imaging. (Fig. 29A) The samples were prepared with and without cells. Since fibrin gel is composed of polypeptide chains, we observed fibrous chain structures. We quantified the fiber density by skeletonizing the SEM image. Images were converted in to 32 bit, and binary mask was obtained. Using binary mask, we skeletonized the image and analyzed. Intriguingly, the samples treated with M2 condition showed sparse and less complex fibrous structure in both conditions compare to the others. (Fig. 29B) It implies that condition medium itself contains matrix metalloproteinase. We confirmed abundant MMP2 and MMP2 expression in M2 CM. (Fig. 30)

We expected the interaction between endothelial cell and cancer cell under CM treatment, however, not significant result observed.

In order to validate the effect of CM on microvessel, we measured the vascular permeability. The device for permeability measurement was described well in our previous research. To validate the effect of tumor on vasculature, we mixed LF and CRC cells at 1:20 ratio. As a result, the vascular permeability coefficient was increased when we introduced CM. Permeability coefficient (P) was described

above.

We measure the fluorescence intensity near the boundary of perivascular and microvessel region. The boundary was represented in white dashed-lines. (Fig 31A) Since we capture the fluorescence images several times with interval, we obtained permeability coefficient.

As a result, vascular permeability increased when we cultured the microvessel with CRC cells together. It seems that cancer cells increased vascular permeability by releasing VEGF-A. This VEGF-mediated hyperpermeability is the major feature of tumor vasculature. In addition, the vascular permeability coefficient was increased even under the LF only condition when CM introduced. (Fig. 30A) In LF only condition, vascular permeability increased in all types of CM, indicating the effect of CM on vascular tight junction itself. Compared to the M0 and M2 treatment, we did not observe significant the differences in all conditions. Especially, there was no significant difference between SW480 and LF only conditions. (Fig. 31C, D) However, compared to the LF only or SW480 condition, hyperpermeability was observed in LoVo condition. (Fig. 31 D) Tumor-vascular network that cultured with LoVo showed exceptionally higher permeability coefficient. This hyperpermeability of microvessel is the distinct feature of tumor vasculature. This leaky and disordered vessel is meaningful since it allows small molecular drugs and immune cells to infiltrate to organs.

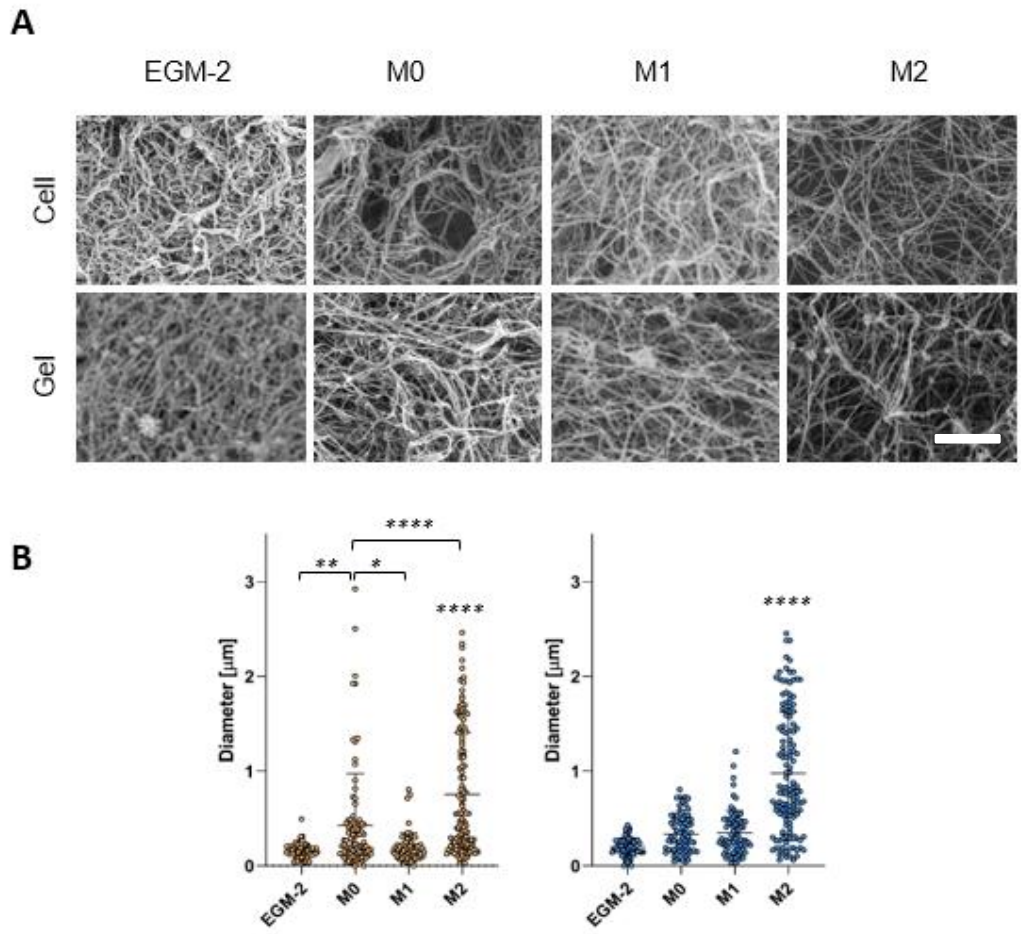


Figure 29. SEM image of extracellular matrix. (A) SEM image of ECM with/without the cells. Scale bar = 3μm (B) Measurement of hole diameter by fibrin fiber. SEM image was converted into binary mask and skeletonized. Analyze particle was used.

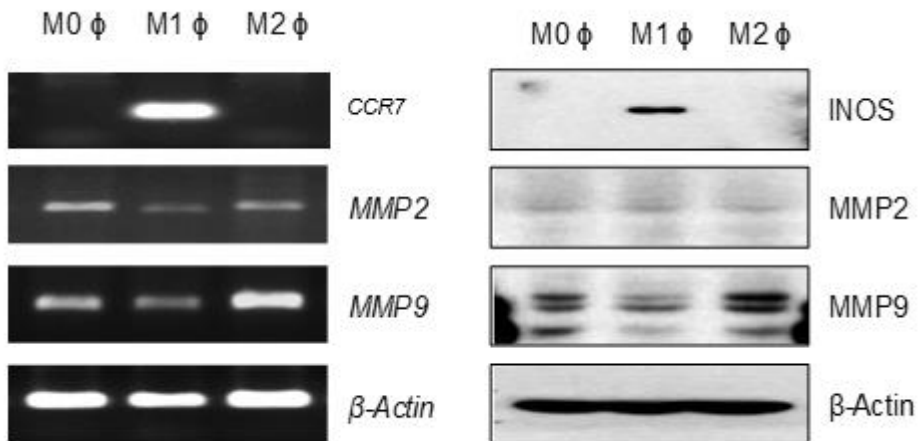


Figure 30. Western blot of Matrix metallopeptidase MMP2 and MMP9. Extracellular matrix was remodeled by macrophage. MM2 and MMP 9 were abundant in M2 macrophage CM

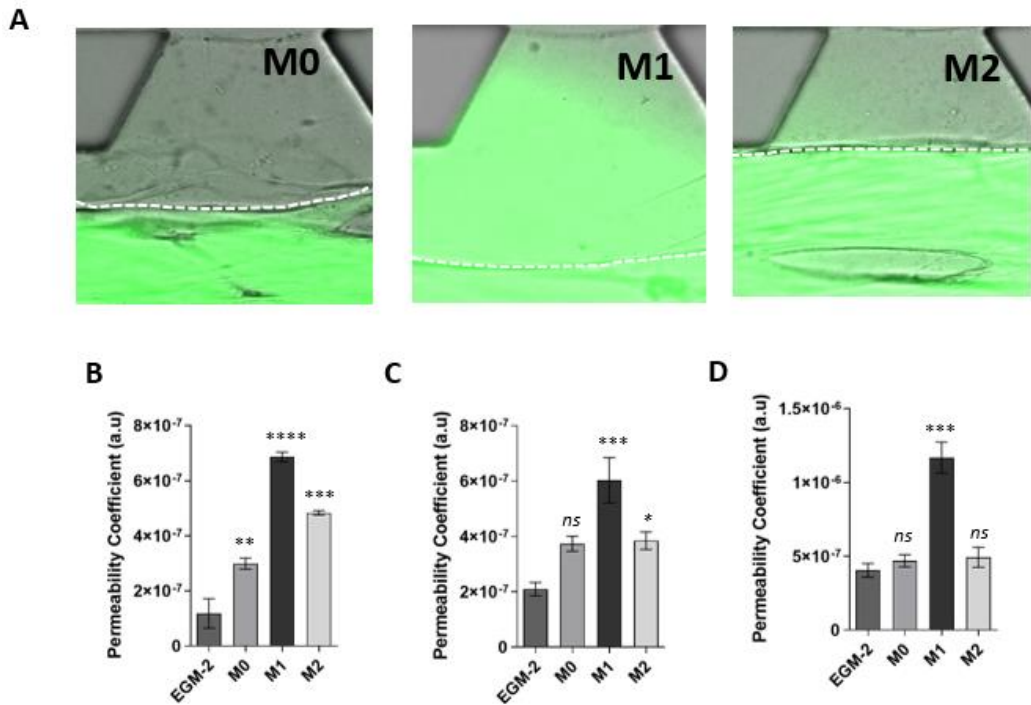


Figure 31. The effect of macrophage on vascular permeability. (A) Permeability coefficient was measured by FITC-dextran. Fluorescence dye is permeable from intravascular region to perivascular region. Time lapse imaging was acquired to measure permeability coefficient. Micro vessels were vascularized with (B) LF only (C) SW480 (D) LoVo.

3-3-3. The effect of macrophage on endothelial tight junctions.

Based on our result, the vascular permeability was increased under the treatment of CM. Therefore, we tried to confirm the vascular tight junction that regulating vascular permeability. There are many tight junctions such as occludin, claudin and VE-Cadherin, these proteins play a key role in regulating interstitial barrier and cell-cell communication.

Especially, TNF- α is known to be a key factor in inflammation initiation and TNF- α signaling pathway is responsible for the expression of adhesion molecules such as Intercellular Adhesion Molecule 1 (ICAM-1) or Vascular cell adhesion protein 1 (VCAM-1) in the endothelium. We though pro-inflammatory M1 CM contains abundant TNF- α and it promotes ICAM-1 upregulation. (Fig. 32) Moreover, phosphorylation ICAM-1 regulates subsequential signaling of VE-cadherin in endothelial cells. Consequently, phosphorylation of VE-cadherin increased and vascular permeability does. The ICAM-1 pathway activation and protein displacement of VE-cadherin according to phosphorylation has been reported recently. This protein displacement makes gaps between endothelial cells and leads an increased in vascular permeability.

As shown in Figure 31 B-D, we observed increased vascular permeability under M1 CM treatment. Therefore, we expected to observe the activation of ICAM-1. We succeed to observe ICAM-1 activation(CD54) in all CM conditions. (Fig. 32)

However, we observed highly expressed VE-cadherin in M1 CM but not in M0 or M2 CM. Moreover, we observed phospho-VE-Cadherin in M1 CM, confirming ICAM-1 and VE cadherin mediated increased vascular permeability.

Moreover, we observed cytokine assay both in cancer monoculture and tumor vascular co-culture condition. As a result, fewer types of inflammatory cytokines were detected in co-culture condition. We just assume that other cells such as endothelial cell and fibroblast consumed the inflammatory cytokines that released from both cancer cell and macrophage.

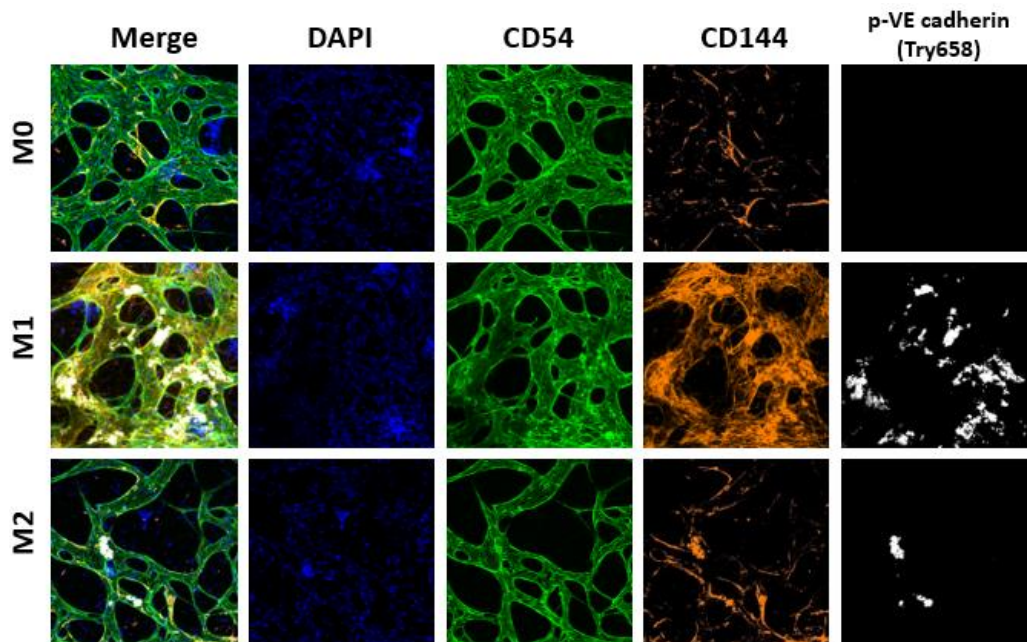


Figure 32. Confocal image of tight junction expression. CD54 and expressed in all condition. CD144 and phosphor VE-cadherin was observed in only M1 condition.

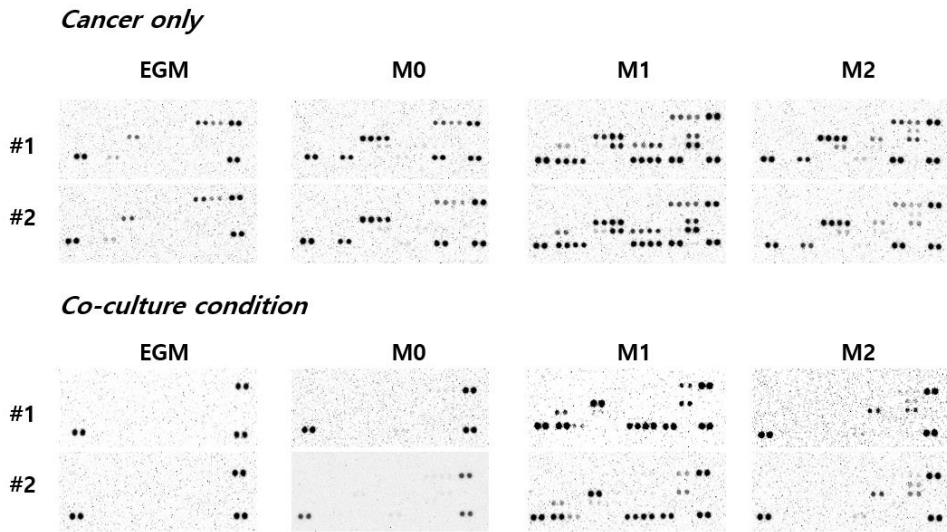


Figure 33. Cytokine assay of cancer monoculture and tumor vessel co-culture condition. Fewer types of inflammatory cytokines were detected in co-culture condition.

3-4. Summary

The subtype classification of macrophages and the role of each subtype in various carcinomas including colorectal cancer have been studied for decades. Moreover, the existence and distribution of macrophages as well as their significance in TME have been studied even at single cell sequencing level. However, consistent results on the role of tumor associated macrophages and their relationship with clinical prognosis have not been elucidated yet. Therefore, there is disagreement about the role of macrophage on carcinoma. As a result of single cell sequencing of normal and tumor tissues of colorectal cancer patients, it was confirmed that the proportion of myeloid cells in the tumor tissues was significantly increased compared to normal, and the proportion of dendritic cells was less than 5%, and macrophages occupied most of myeloid cells. Therefore, the study of the role of macrophages in colon cancer has become more important. Recently, while research on immunotherapy is actively being conducted, in the case of colorectal cancer, the overall response rate(ORR) for PD-1 and PD-L1, which are representative anti-cancer immunotherapy drugs, is less than 40%, and in the case of MSI, which accounts for 85% of colorectal cancer, pembrolizomab The ORR for was reported as 0%. (2015 NEJM) We proposed our novel *in vitro* tumor-vascular models to evaluate the role of macrophage on not only tumor progression but also the tumor

microenvironment. We validated the effect of macrophage on colorectal cancer cells. As a result, M1 macrophage represent pro-inflammatory effect where as M2 macrophage induced tumor progression. M2 macrophage also contributed to ECM remodeling by secreting MMPs. Meanwhile, we measured vascular permeability and confirmed that M1 macrophage increased vascular permeability by phosphorylation of VE-cadherin. There has been no significant result in SW480 and LoVo as a representative of MSS and MSI classification respectively. However, our model is still expected to use as a powerful preclinical model to evaluate the colorectal cancer immunotherapy.

4. Conclusion

A number of models for colorectal cancer study have been developed, however, there is still lack of adequate model. Colorectal cancer is highly metastatic cancer and liver is the most common site of metastasis. This distance metastasis occurs via blood vessel that flow from colon to liver. Therefore, more complex model considering tumor vessel are required.

We developed high-throughput in vitro tumor vessel array for evaluation of anti-cancer drugs or cancer-immunotherapy. Cancer immunotherapy becomes promising candidate in cancer treatment. However, the understanding of interaction between immune cells and tumor cells remains poorly understood. In this thesis, we reconstruct tumor microvessel with various colorectal cancer subtypes and examined the cytotoxic activity of NK cells. We confirmed the different behavior of NK cells according to colorectal cancer CMS classifications.

Meanwhile, tumor-associated macrophage holds a great potential in cancer immunotherapy. As a result of single cell sequencing of normal and tumor tissues of colorectal cancer patients, it was confirmed that the proportion of myeloid cells in the tumor tissues was significantly increased compared to normal, and the proportion of dendritic cells was less than 5%, and macrophages occupied

most of myeloid cells. However, consistent results on the role of tumor associated macrophages and their relationship with clinical prognosis have not been elucidated yet. We verified the role of macrophage on colorectal cancer according to their subtypes. We confirmed M1 macrophage represent anti-tumor behavior whereas, M2 macrophage prompt tumor progression and involved in ECM remodeling. We also verified the effect of M1 macrophage on vascular permeability and vessel junction. We expect our model to help understanding cancer and interaction between cancer and immune cell *in vitro*.

References

1. Kato Y., et al., *Acidic extracellular microenvironment and cancer*. Cancer Cell International 2013.
2. Nanashima A., et al., *Analysis of tumor morphology in metastatic colorectal cancer: does this classification have any clinical significance??* J Gastroenterol 2002.
3. *Cancer Facts & Figures*. American Cancer Society, 2019.
4. Jain, R.K., *Normalization of Tumor Vasculature: An Emerging Concept in Antiangiogenic Therapy*. SCIENCE, 2005.
5. Lee Y., et al., *Crosstalk between CCL7 and CCR3 promotes metastasis of colon* Oncotarget, 2016.
6. Klampfer, L., *CYTOKINES, INFLAMMATION AND COLON CANCER*. Curr Cancer Drug Targets, 2011.
7. Yang, Y., et al., *GSTpi regulates VE-cadherin stabilization through promoting S-glutathionylation of Src*. Redox Biol, 2020. **30**: p. 101416.
8. Zervantonakis, I.K., et al., *Three-dimensional microfluidic model for tumor cell intravasation and endothelial barrier function*. Proc Natl Acad Sci U S A, 2012. **109**(34): p. 13515-20.
9. Oh B., et al., *Twist1-induced epithelial-mesenchymal transition according to microsatellite instability status in colon cancer cells*. 2016.
10. Jessie S. Jeona, et al., *Correction for Jeon et al., Human 3D vascularized organotypic microfluidic assays to study breast cancer cell extravasation*. Proceedings of the National Academy of Sciences, 2015. **112**(7): p. E818-E818.
11. Ahn, J., et al., *Microfluidics in nanoparticle drug delivery; From synthesis to pre-clinical screening*. Adv Drug Deliv Rev, 2018. **128**: p. 29-53.
12. Allen, S.G., et al., *Macrophages Enhance Migration in Inflammatory Breast Cancer Cells via RhoC GTPase Signaling*. Sci Rep, 2016. **6**: p. 39190.
13. Ayuso, J.M., et al., *Evaluating natural killer cell cytotoxicity against solid tumors using a microfluidic model*. Oncoimmunology, 2019. **8**(3): p. 1553477.
14. Azzi, S., J.K. Hebda, and J. Gavard, *Vascular permeability and drug delivery in cancers*. Front Oncol, 2013. **3**: p. 211.
15. Berg, K.C.G., et al., *Multi-omics of 34 colorectal cancer cell lines - a resource for biomedical studies*. Mol Cancer, 2017. **16**(1): p. 116.
16. Bernot, D., et al., *Upregulation of TNF-alpha-induced ICAM-1 surface expression by adenylate cyclase-dependent pathway in human endothelial cells*. J Cell Physiol, 2005. **202**(2): p. 434-41.

17. Berry, S.B., et al., *Droplet Incubation and Splitting in Open Microfluidic Channels*. Anal Methods, 2019. **11**(35): p. 4528-4536.
18. Bi, Y., et al., *Tumor-on-a-chip platform to interrogate the role of macrophages in tumor progression*. Integr Biol (Camb), 2020. **12**(9): p. 221-232.
19. Boussommier-Calleja, A., et al., *The effects of monocytes on tumor cell extravasation in a 3D vascularized microfluidic model*. Biomaterials, 2019. **198**: p. 180-193.
20. Cassetta, L. and T. Kitamura, *Macrophage targeting: opening new possibilities for cancer immunotherapy*. Immunology, 2018. **155**(3): p. 285-293.
21. Choo, Y.W., et al., *M1 Macrophage-Derived Nanovesicles Potentiate the Anticancer Efficacy of Immune Checkpoint Inhibitors*. ACS Nano, 2018. **12**(9): p. 8977-8993.
22. Chow, F.C. and K.S. Chok, *Colorectal liver metastases: An update on multidisciplinary approach*. World J Hepatol, 2019. **11**(2): p. 150-172.
23. Fisher, R.A., *Anonymous live liver donor: the Good Samaritan Stranger*. Nat Rev Gastroenterol Hepatol, 2019. **16**(11): p. 650-651.
24. Gebala, V., et al., *Blood flow drives lumen formation by inverse membrane blebbing during angiogenesis in vivo*. Nat Cell Biol, 2016. **18**(4): p. 443-50.
25. Genin, M., et al., *M1 and M2 macrophages derived from THP-1 cells differentially modulate the response of cancer cells to etoposide*. BMC Cancer, 2015. **15**: p. 577.
26. Giannotta, M., M. Trani, and E. Dejana, *VE-cadherin and endothelial adherens junctions: active guardians of vascular integrity*. Dev Cell, 2013. **26**(5): p. 441-54.
27. Gurevich, D.B., et al., *Live imaging of wound angiogenesis reveals macrophage orchestrated vessel sprouting and regression*. EMBO J, 2018. **37**(13).
28. Haase, K., et al., *Endothelial Regulation of Drug Transport in a 3D Vascularized Tumor Model*. Advanced Functional Materials, 2020: p. 2002444.
29. Hsu, T.H., et al., *The migration speed of cancer cells influenced by macrophages and myofibroblasts co-cultured in a microfluidic chip*. Integr Biol (Camb), 2012. **4**(2): p. 177-82.
30. Hu, W., et al., *Cancer Immunotherapy Based on Natural Killer Cells: Current Progress and New Opportunities*. Front Immunol, 2019. **10**: p. 1205.
31. Inamura, K., *Colorectal Cancers: An Update on Their Molecular Pathology*. Cancers (Basel), 2018. **10**(1).
32. Junttila, M.R. and F.J. de Sauvage, *Influence of tumour micro-environment heterogeneity on therapeutic response*. Nature, 2013. **501**(7467): p. 346-54.
33. Kim, H., et al., *Macrophages-Triggered Sequential Remodeling of*

- Endothelium-Interstitial Matrix to Form Pre-Metastatic Niche in Microfluidic Tumor Microenvironment*. Adv Sci (Weinh), 2019. **6**(11): p. 1900195.
34. Kim, S., et al., *Vasculature-On-A-Chip for In Vitro Disease Models*. Bioengineering (Basel), 2017. **4**(1).
 35. Ko, J., et al., *Tumor spheroid-on-a-chip: a standardized microfluidic culture platform for investigating tumor angiogenesis*. Lab Chip, 2019. **19**(17): p. 2822-2833.
 36. Lee, D.H., et al., *An integrated microfluidic platform for size-selective single-cell trapping of monocytes from blood*. Biomicrofluidics, 2018. **12**(5): p. 054104.
 37. Lee, H., et al., *A bioengineered array of 3D microvessels for vascular permeability assay*. Microvasc Res, 2014. **91**: p. 90-8.
 38. Lee, S.W.L., et al., *Characterizing the Role of Monocytes in T Cell Cancer Immunotherapy Using a 3D Microfluidic Model*. Front Immunol, 2018. **9**: p. 416.
 39. Lee, S.W.L., et al., *Integrated in silico and 3D in vitro model of macrophage migration in response to physical and chemical factors in the tumor microenvironment*. bioRxiv, 2020.
 40. Li, R., et al., *Macrophage-Secreted TNFalpha and TGFbeta1 Influence Migration Speed and Persistence of Cancer Cells in 3D Tissue Culture via Independent Pathways*. Cancer Res, 2017. **77**(2): p. 279-290.
 41. Liu, Y., et al., *Human in vitro vascularized micro-organ and micro-tumor models are reproducible organ-on-a-chip platforms for studies of anticancer drugs*. Toxicology, 2020. **445**: p. 152601.
 42. Mager, L.F., et al., *Cytokine-Induced Modulation of Colorectal Cancer*. Front Oncol, 2016. **6**: p. 96.
 43. Mantovani, A. and P. Allavena, *The interaction of anticancer therapies with tumor-associated macrophages*. J Exp Med, 2015. **212**(4): p. 435-45.
 44. Michna, R., et al., *Vascularized microfluidic platforms to mimic the tumor microenvironment*. Biotechnol Bioeng, 2018. **115**(11): p. 2793-2806.
 45. Miyazaki, K., et al., *Establishment of a method for evaluating endothelial cell injury by TNF-alpha in vitro for clarifying the pathophysiology of virus-associated acute encephalopathy*. Pediatr Res, 2017. **81**(6): p. 942-947.
 46. Munos, B., *Lessons from 60 years of pharmaceutical innovation*. Nat Rev Drug Discov, 2009. **8**(12): p. 959-68.
 47. Nagtegaal, I.D. and H.J. Schmol, *Colorectal cancer: What is the role of lymph node metastases in the progression of colorectal cancer?* Nat Rev Gastroenterol Hepatol, 2017. **14**(11): p. 633-634.
 48. Narayanan, S., et al., *Tumor Infiltrating Lymphocytes and Macrophages Improve Survival in Microsatellite Unstable Colorectal Cancer*. Sci Rep, 2019. **9**(1): p. 13455.

49. Palomba, R., et al., *Biomimetic carriers mimicking leukocyte plasma membrane to increase tumor vasculature permeability*. *Sci Rep*, 2016. **6**: p. 34422.
50. Park, D., et al., *High-Throughput Microfluidic 3D Cytotoxicity Assay for Cancer Immunotherapy (CACI-IMPACT Platform)*. *Front Immunol*, 2019. **10**: p. 1133.
51. Park, J., et al., *Chemotaxis of Lipopolysaccharide-Stimulated RAW264.7 Macrophage Cell Line in Microfluidic Channels*. *Journal of Nanoscience and Nanotechnology*, 2017. **17**(11): p. 7996-8000.
52. Phan, D.T.T., et al., *A vascularized and perfused organ-on-a-chip platform for large-scale drug screening applications*. *Lab Chip*, 2017. **17**(3): p. 511-520.
53. Romero-Lopez, M., et al., *Recapitulating the human tumor microenvironment: Colon tumor-derived extracellular matrix promotes angiogenesis and tumor cell growth*. *Biomaterials*, 2017. **116**: p. 118-129.
54. Schaaf, M.B., A.D. Garg, and P. Agostinis, *Defining the role of the tumor vasculature in antitumor immunity and immunotherapy*. *Cell Death Dis*, 2018. **9**(2): p. 115.
55. Schildberger, A., et al., *Monocytes, peripheral blood mononuclear cells, and THP-1 cells exhibit different cytokine expression patterns following stimulation with lipopolysaccharide*. *Mediators Inflamm*, 2013. **2013**: p. 697972.
56. Song, J.W., et al., *Microfluidic endothelium for studying the intravascular adhesion of metastatic breast cancer cells*. *PLoS One*, 2009. **4**(6): p. e5756.
57. Sticker, D., et al., *Microfluidic Migration and Wound Healing Assay Based on Mechanically Induced Injuries of Defined and Highly Reproducible Areas*. *Anal Chem*, 2017. **89**(4): p. 2326-2333.
58. Tsai, H.-F., et al., *Tumour-on-a-chip: microfluidic models of tumour morphology, growth and microenvironment*. *Journal of The Royal Society Interface*, 2017. **14**(131): p. 20170137.
59. Yan, M., et al., *Endothelial cell SHP-2 negatively regulates neutrophil adhesion and promotes transmigration by enhancing ICAM-1-VE-cadherin interaction*. *FASEB J*, 2017. **31**(11): p. 4759-4769.
60. Yang, Y., et al., *GSTpi regulates VE-cadherin stabilization through promoting S-glutathionylation of Src*. *Redox Biol*, 2020. **30**: p. 101416.
61. Zervantonakis, I.K., et al., *Three-dimensional microfluidic model for tumor cell intravasation and endothelial barrier function*. *Proc Natl Acad Sci U S A*, 2012. **109**(34): p. 13515-20.

초 록

대장암은 전체 사망률 2위에 해당하는 중대한 질병이다. 특히 대장암은 간으로 직접적으로 이어지는 혈관인 간문맥(Portal vein)을 따라 가장 빈번하게 전이가 일어나는 질병이기 때문에 대장암의 연구에 있어 주변 혈관에 관한 연구는 더욱 중요성이 크다. 하지만 현재까지 암-혈관에 관련된 연구는 이종이식을 통한 연구에 많이 치우쳐 있다. 이종이식을 통한 연구는 짧게는 수 주에서 수 개월이 걸리고 그 시간과 비용이 막대하다. 뿐만 아니라 사람과 동물이라는 이종간의 계통발생학적 차이라는 한계가 있다. 이를 극복하기 위하여 마이크로 공학을 이용한 다양한 체외 모델들이 제시되고 있으나, 여전히 낮은 효율과 실험자의 높은 숙련도를 요구한다. 이에 본 연구는 플라스틱 사출 성형 기반 디바이스를 이용하여 고효율 암 혈관 미세환경을 구현하고자 하였다. 레일 가이드 고속 유체 패터닝 기술을 이용하여 누구나 쉽게 3차원 세포 배양을 가능하도록 하였으며, 적은 양의 세포와 배양액만으로도 5일 이내에 관류 가능한 암-혈관 공배양 시스템을 구현할 수 있는 최적의 조건을 확립하였다. 또한 정상혈관 대비 암혈관의 두드러진 특성에 대하여 형태적 기능적인 검증을 통해 유효성을 확인하였으며, 그 결과 암혈관은 정상혈관 대비 혈관의 투과성이 현저히 높아지는 것을 보였다. 이에 면역세포의 일종인 자연살해세포를 이용하여 면역세포의 혈관을 통한 면역감시체계를 구현해 냈으며, 장기간 라이브 이미징 기술을 이용하여 자연살해세포의 혈관밖 유출 및 유입 그리고 대장암의 암종별 세포독성에 대한 평가를 수행하였다. 자연살해세포는 대장암 암종별에 따라 서로 다른 혈관 밖 유입률 및 세포독성을 보였으며 이는 임상적으로 유의미한 결과라고 볼 수 있다. 뿐만 아니라 림프구의 일종인 대식세포를 이용하여, 대식세포의 분화에 따른 암-혈관 미세환경에 미치는 영향에 대한 평가를 수행하였다. 그 결과 대식세포는 분화에 따른 아형에 따라 암세포의 자살을 유도하거나 반대로 암세포의 진행을 유도하기도 하는 서로 다른 특성을 갖는 것 뿐만

아니라 혈관의 투과성 및 주변 세포외기질의 변화에도 영향을 미치는 것을 체외에서 확인하였다. 대식세포는 전체 림프구를 구성하는 면역세포 중 85퍼센트를 차지하는 세포로 자연살해세포와 더불어 차세대 면역세포 치료제로서의 가능성이 매우 높다. 본 연구를 통해 개발된 모델은 관류 가능한 암-혈관 시스템을 통하여 매년 새롭게 개발되는 항암 신약 뿐만 아니라 면역세포치료제의 평가 플랫폼으로써 무한한 활용 가능성을 지닌다고 볼 수 있다.